Correlating Thermodynamic and Kinetic Hydricities of Rhenium Hydrides

Matthew R. Espinosa,[a] Mehmed Z. Ertem,[b,*] Mariam Barakat,[c] Quinton J. Bruch,[d] Anthony P. Deziel,[a] Matthew R. Elsby,[a] Faraj Hasanayn,[c] Nilay Hazari,[a,*] Alexander J. M. Miller,[d,*] Matthew V. Pecoraro,[a] Allison M. Smith,[d] & Nicholas E. Smith[a]

[a]Department of Chemistry, Yale University, P. O. Box 208107, New Haven, Connecticut, 06520, USA. E-mail: nilay.hazari@yale.edu

[b]Chemistry Division, Brookhaven National Laboratory, Upton, New York, 11973, USA. E-mail: mzertem@bnl.gov

[c]Department of Chemistry, American University of Beirut, Beirut 1107 2020, Lebanon.

[d]Department of Chemistry, University of North Carolina at Chapel Hill, Chapel Hill, North Carolina, 27599, USA. E-mail: ajmm@email.unc.edu

Abstract

The kinetics of hydride transfer from Re(^{R}bpy)(CO)$_3$H (bpy = 4,4'-R-2,2'-bipyridine; R = OMe, ^{t}Bu, Me, H, Br, COOMe, CF$_3$) to CO_2 and seven different cationic N-heterocycles were determined. Additionally, the thermodynamic hydricities of complexes of the type Re(^{R}bpy)(CO)$_3$H were established primarily using computational methods. Linear Free Energy Relationships (LFERs) derived by correlating thermodynamic and kinetic hydricities indicate that, in general, the rate of hydride transfer increases as the thermodynamic driving force for the reaction increases. Kinetic isotope effects range from inverse for hydride transfer reactions with a small driving force to normal for reactions with a large driving force. Hammett analysis indicates that hydride transfer reactions with greater thermodynamic driving force are less sensitive to changes in the electronic properties of the metal hydride, presumably because there is less build-up of charge in the increasingly early transition state. Bronsted α values were obtained for a range of hydride transfer reactions and along with DFT calculations suggest the reactions are concerted, which enables the use of Marcus theory to analyze hydride transfer reactions involving transition metal hydrides. It is notable, however, that even slight perturbations in the steric properties of the Re hydride or the hydride acceptor result in large deviations in the predicted rate of hydride transfer based on thermodynamic driving forces. This indicates that thermodynamic considerations alone cannot be used to predict the rate of hydride transfer, which has implications for catalyst design.

Introduction

Transition metal hydrides are crucial intermediates in a plethora of catalytic reactions, including reactions relevant to: (i) energy storage applications,[1] (ii) the synthesis of pharmaceuticals [2,3,4] and (iii) the preparation of monomers for polymerization.[5] In many of these reactions, hydride transfer (either from a transition metal hydride to a substrate or from a substrate to a transition metal to form a transition metal hydride) is the turnover-limiting step. Therefore, an increased understanding of hydride transfer with transition metals as either the hydride donor or acceptor is critical for the design of efficient catalysts for current and new reactions.

Two different approaches have traditionally been utilized to quantify the ability of a transition metal hydride to donate a hydride. *Thermodynamic hydricity* is the free energy required to release a hydride ion, H^-, from a species in solution (ΔG^o_{H-}) (Figure 1A).[6] It is a thermodynamic parameter and quantifies the driving force for hydride transfer. Thermodynamic hydricity is valuable for understanding observed reactivity or selectivity, and for predicting if a hydride transfer reaction will be favorable, but it often cannot provide insight into catalytic activity. *Kinetic hydricity* is the elementary rate constant for a particular hydride transfer reaction and is related to the free energy of activation ($\Delta G^{\ddagger}_{H-}$) (Figure 1B).[6b,6e] Studies of kinetic hydricity offer information on the barriers for hydride transfer from a catalyst to a hydride acceptor and can establish whether that step is turnover-limiting and how to accelerate it. While the importance of thermodynamic and kinetic hydricity are well established,[6] the paucity of cases where *both* thermodynamic and kinetic hydricity have been measured for the same transition metal hydride is striking.[6e] This void is likely because thermodynamic and kinetic hydricity are often challenging to measure experimentally, which means that finding a system where it is possible to determine both is not straightforward.

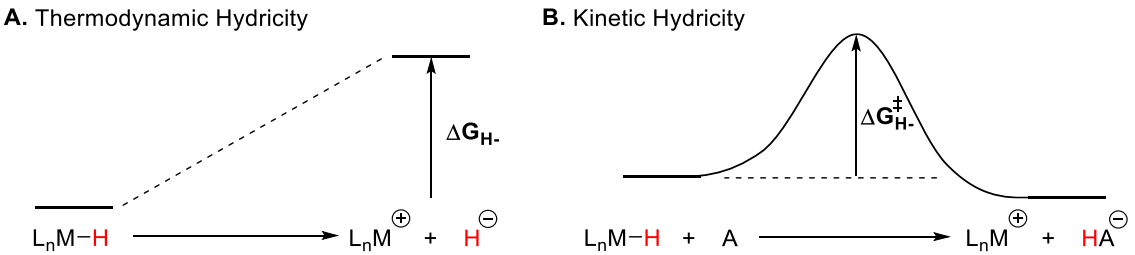

Figure 1: Representations of: (**A**) Thermodynamic hydricity, which is the Gibbs free energy difference between a metal hydride (L_nM-H) and the product of bond scission (L_nM^+ *and* H^-). The definition includes non-specific solvation effects, as well as the energy of any solvent binding to the metal center. (**B**) Kinetic hydricity, which is the elementary rate constant for a hydride transfer reaction from a metal hydride (L_nM-H) to a hydride acceptor (A). It is related to the activation energy ($\Delta G^{\ddagger}_{H-}$) for hydride transfer.

Linear free-energy relationships (LFERs), which correlate thermodynamic and kinetic parameters, are a common tool for catalyst design.[7] However, given the absence of thermodynamic and kinetic hydricity measurements on the same system, there are few examples of LFERs for hydride transfer reactions involving metal hydrides. This stands in contrast to hydride transfer reactions between two organic substrates, where LFERs between the rate of hydride transfer and the equilibrium constants for exchange between the organic hydride donor and acceptor (which is a surrogate for relative thermodynamic hydricity) are common.[6c,8] These LFERs hold for a range of hydride donors and acceptors and have been used to show that Marcus theory can be used to analyze hydride transfer between organic substrates.[8a-e,8i,9] Directly connecting results from organic hydrides to transition metal hydrides, however, is challenging because metal hydrides are often larger, have more variations in electronic structure and mechanistic pathways, and are capable of binding acceptors after hydride transfer. Thus, to create LFERs for metal hydrides there is an unmet need to understand these factors.

Currently, the most robust experimental LFERs involving thermodynamic hydricity of transition metal hydrides have entailed correlations with catalytic activity, as determined by the turnover frequency (TOF), rather than with a measured rate constant for an elementary step involving hydride transfer. For instance, Wiedner, Linehan, and co-workers showed that in CO_2 hydrogenation to formate using Co hydride catalysts, there is a strong correlation between the thermodynamic hydricity of the Co hydride and the TOF.[10] Similarly, Ngo and Do demonstrated that the catalytic activity of a series of Cp*Ir-based hydrides for the transfer hydrogenation of benzaldehyde to benzyl alcohol using sodium formate as the hydrogen source correlates with their thermodynamic hydricity.[11] In cases where hydride transfer is the turnover-limiting step in catalysis, these correlations between thermodynamic hydricity and TOF can be used as proxies for determining the relationship between thermodynamic and kinetic hydricity. However, despite their utility in predicting catalytic activity for a specific reaction, the relationships cannot be generalized to other substrates or readily used to develop a unified model for hydride transfer.

To develop a general model for hydride transfer involving transition metal complexes, it is essential to correlate explicitly kinetic and thermodynamic hydricity across a range of substrates.[6e] The most prominent experimental example of the quantitative correlation of individual hydride transfer kinetics and thermodynamic hydricity for a transition metal hydride was performed by

Matsubara, Muckerman, Creutz, and co-workers.[12] Their results suggest that in hydride transfer reactions from $[Ru(tpy)(bpy)H]^+$ (tpy = 2,2';6',2''-terpyridine; bpy = 2,2'-bipyridine) to five different cationic pyridinium acceptors and CO_2 (Figure 2A), there is a linear relationship between thermodynamic and kinetic hydricity, which implies that the rate of hydride transfer increases as the driving force for the reaction increases. However, problems with solubility and the measurement of kinetics prevented quantitative data from being obtained under the same conditions for most of the acceptors and no changes were made to the Ru complex, both of which limit the generality of their results. Faster hydride transfer was also observed with greater driving force in independent studies by Bullock *et al.* and Bruno *et al.* examining hydride transfer from several metal hydrides to a trityl cation acceptor (Figure 2B).[13] Nevertheless, when Bruno *et al.*

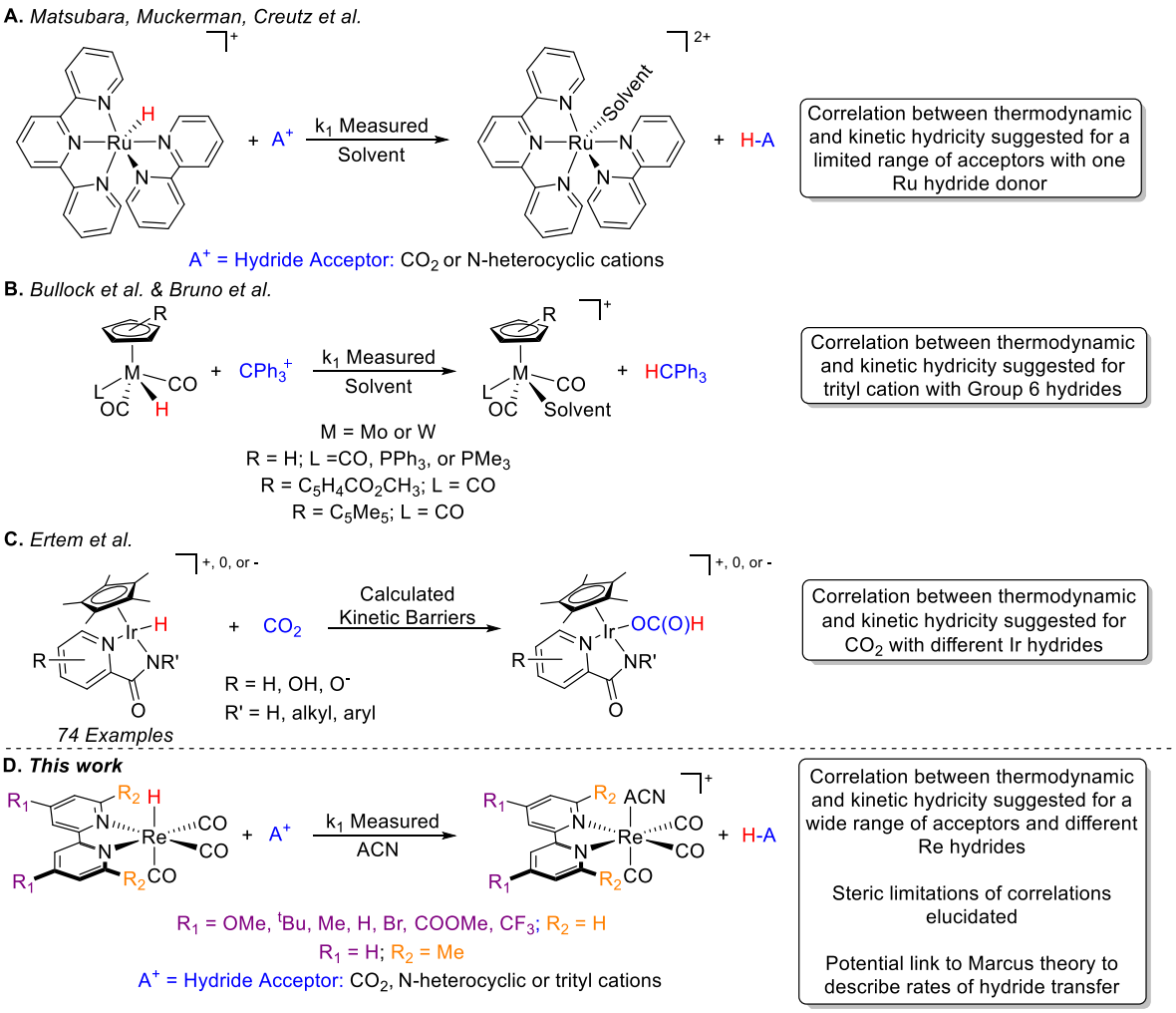

Figure 2: (**A-C**) Previous work that suggests a relationship between thermodynamic hydricity and kinetic hydricity for a single elementary step. (**D**) This work develops LFERs for hydride transfer from $Re(^{R}bpy)(CO)_3H$ to CO_2 and cationic N-heterocycles that differ in thermodynamic hydricity by 35 kcal mol^{-1}. The results show there is a clear correlation between thermodynamic and kinetic hydricity. ACN = acetonitrile.

attempted to correlate the rates of hydride transfer to the equilibrium constants for exchange, as has been performed for organic hydride reactions, they were unable to accurately determine the equilibrium constants preventing the construction of a quantitative LFER.[14] More recently, Ertem and co-workers calculated the thermodynamic and kinetic hydricities of 74 complexes of the form $[Cp^*Ir(L)(H)]^q$ (q = –1, 0, +1) (Figure 2C).[15] Their computations predicted that as the thermodynamic hydricity of the hydrides increased, the kinetics ($\Delta G^{\ddagger}$) of electrophilic CO_2 attack on the iridium hydride species would accelerate. Although all of these studies suggest the same conclusion, the hydride acceptors employed are not structurally diverse and do not span a wide range of hydride acceptor abilities,[16] which prevents conclusions about how the nature of the hydride acceptor impacts the reactions. For example, the sensitivity of measurements to steric factors is unclear and it is unknown if a correlation between thermodynamic and kinetic hydricity for CO_2 will be relevant to the correlation for a pyridinium cation (or other hydride acceptors). This prevents the transfer of results from one substrate to another substrate in catalysis.

In this work, we quantify the ability of a series of electronically diverse, but sterically similar Re hydrides to transfer a hydride to a range of organic acceptors (Figure 2D). In fact, by modifying the hydride acceptor we both alter the thermodynamics of hydride transfer by 35 kcal mol^{-1} and measure hydride transfer under diverse steric conditions. This allows us to establish LFERs between the kinetics of hydride transfer from the metal hydrides to a given hydride acceptor and the thermodynamic hydricity of the different Re hydrides. We show that the conventional wisdom that more hydridic metal hydrides will undergo faster hydride transfer is correct only under certain conditions, and is especially problematic when varying both the identity of the metal hydride donor and acceptor. Mechanistic studies provide evidence for a concerted hydride transfer from the metal to the acceptor, but in some cases the thermodynamics of the product of hydride transfer binding to the metal center need to be considered to account for trends in rates across different hydride acceptors. Our large data set enables us to demonstrate that it is possible to use Marcus theory to interpret the rates of hydride transfer for particular metal hydride/organic acceptor pairs and we estimate the reorganization energy for some hydride transfer reactions. Overall, the kinetic and thermodynamic analyses detailed herein provide guidance on when different strategies are appropriate for predictive design of catalysts or reaction conditions to promote or inhibit hydride transfer from metal hydrides.

Results and Discussion

Experimental Measurements of Kinetic Hydricity

To explore the correlation between kinetic and thermodynamic hydricity we synthesized electronically varied Re hydrides of the form Re(^{R}bpy)(CO)$_3$H (^{R}bpy = 4,4'-R-2,2'-bipyridine; R = OMe, ^{t}Bu, Me, H, Br, COOMe, and CF$_3$, see section SII). These complexes were selected for synthetic ease and because it was previously demonstrated that the kinetics of CO_2 insertion to form formate complexes of the type Re(^{R}bpy)(CO)$_3${OC(O)H} can be measured for some of these hydrides.[17] Although referred to as CO_2 insertion reactions, the first step of these reactions is likely rate-determining outer-sphere hydride transfer[18] to CO_2 (Figure 3 & *vide infra*), and therefore the measured rates reflect the kinetic hydricity of the transition metal hydride.[19] We determined the kinetics of CO_2 insertion into Re(^{R}bpy)(CO)$_3$H in acetonitrile (ACN) using UV-Vis spectroscopy with an excess of CO_2 (0.257 M in ACN at 30 °C) to ensure pseudo-first-order conditions (Figure 3). Representative kinetic traces where the first three half-lives of the reaction are used to determine the rate constant are shown in Figure S2. As observed previously, these reactions are first-order in [Re] and [CO_2], so the overall rate law is rate = k_1[Re(^{R}bpy)(CO)$_3$H][CO_2] (see Figure S3).[17] Values of k_1 for each reaction were obtained by dividing the k_{obs} value from a plot of

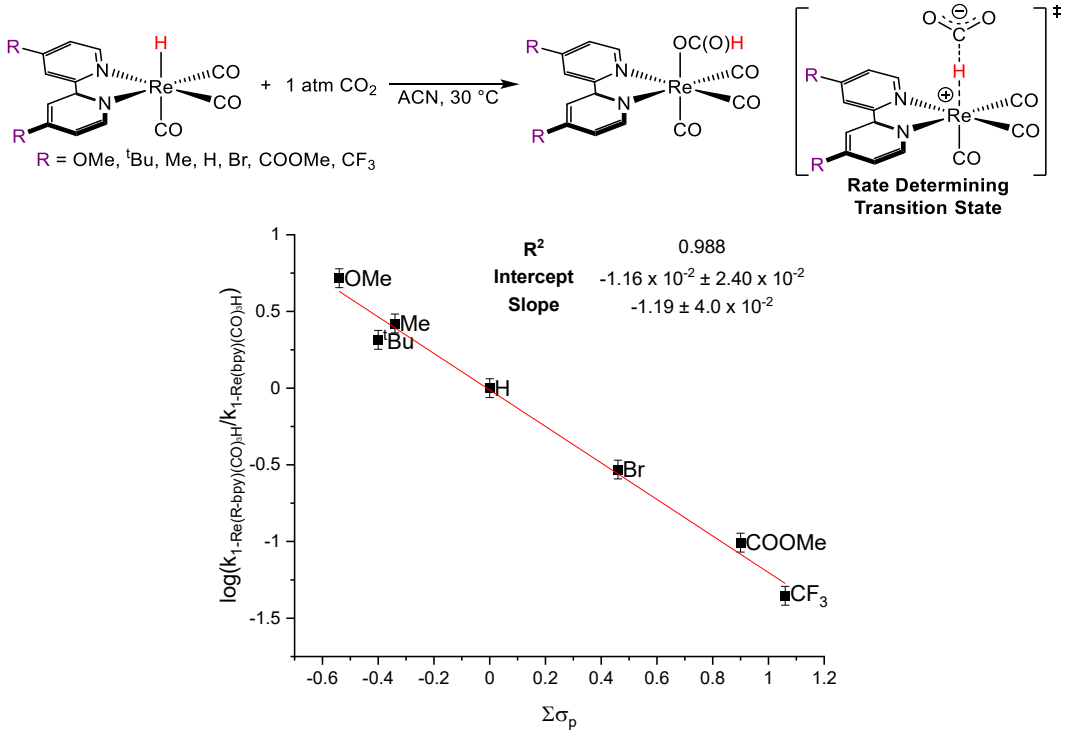

Figure 3: Hammett plot for CO_2 insertion into Re(^{R}bpy)(CO)$_3$H. Reaction conditions: [Re(^{R}bpy)(CO)$_3$H]: ~0.3 mM, [CO_2]: 0.257 M, ACN, 30 °C.

ln([Re(^{R}bpy)(CO)$_3$H] versus time by the concentration of CO_2. The concentration of CO_2 in ACN was determined using quantitative ^{13}C NMR spectroscopy (see section SV).

A Hammett plot was generated for the insertion of CO_2 into our electronically diverse Re hydrides (Figure 3). We used a summed Hammett parameter to account for the disubstituted bpy, and the best correlation was obtained using $\Sigma\sigma_p$, but the summed parameters $\Sigma\sigma_p^+$ and $\Sigma\sigma_p^-$ also give excellent correlations (see Figures S5-S7).[20] A negative slope of –1.19 is observed in the Hammett plot, suggesting a positive charge build-up on the Re center in the transition state (TS) supporting an outer-sphere rate-determining step for CO_2 insertion, which is stabilized by more electron-rich ligands. In fact, there is a difference in the elementary rate constant for CO_2 insertion of more than two orders of magnitude between our most electron-donating hydride (Re(^{OMe}bpy)(CO)$_3$H) and our least electron-donating hydride (Re(^{CF_3}bpy)(CO)$_3$H) indicating the profound influence of electronic factors on this reaction. Our results demonstrate a strong linear correlation between the Hammett parameter and kinetic hydricity. Given that previous work by Miller *et al.* demonstrated a strong linear correlation between the Hammett parameter and thermodynamic hydricity of (distinct) metal hydrides,[21] this is suggestive of a LFER between kinetic and thermodynamic hydricity (*vide infra*).

To gain further information about CO_2 insertion into our family of Re hydrides, the activation parameters for insertion were determined using Eyring analysis (Table 1). Negative entropies were found for all of the insertion reactions, indicating a highly organized rate-limiting TS, in agreement with an outer-sphere CO_2 insertion mechanism where two molecules combine to form one species.[19e-g] The entropic unfavorability of these CO_2 insertion reactions, –33 to –49 cal mol^{-1} K^{-1}, is larger than other examples of CO_2 insertion into metal hydrides, which range from –10 to –35 cal mol^{-1} K^{-1}, suggesting that there may be a stronger interaction between the hydride and the

Table 1: Activation parameters for CO_2 insertion into Re(^{R}bpy)(CO)$_3$H in ACN at 30 °C.

Entry	Complex	$\Delta H^{\ddagger}$ (kcal mol^{-1})	$\Delta S^{\ddagger}$ (cal mol^{-1} K^{-1})	$\Delta G^{\ddagger}_{303}$ (kcal mol^{-1})	$\Delta\Delta G^{\ddagger}_{303}$ (kcal mol^{-1})[a]
1	Re(^{OMe}bpy)(CO)$_3$H	3.8 ± 0.7	-48.9 ± 2.0	18.7 ± 0.5	-0.9
2	Re(^{tBu}bpy)(CO)$_3$H	6.0 ± 0.7	-43.4 ± 2.0	19.1 ± 0.5	-0.5
3	Re(^{Me}bpy)(CO)$_3$H	5.0 ± 0.7	-46.3 ± 2.0	19.1 ± 0.5	-0.5
4	Re(bpy)(CO)$_3$H	7.1 ± 0.7	-41.3 ± 2.0	19.6 ± 0.5	0
5	Re(^{Br}bpy)(CO)$_3$H	10.2 ± 0.9	-33.4 ± 2.8	20.3 ± 0.6	0.7
6	Re(^{COOMe}bpy)(CO)$_3$H	8.8 ± 0.7	-40.2 ± 2.0	21.0 ± 0.6	1.4
7	Re(^{CF_3}bpy)(CO)$_3$H	8.9 ± 0.3	-41.4 ± 2.0	21.5 ± 0.6	1.9

[a]Obtained by subtracting the value of $\Delta G^{\ddagger}_{303}$ for a particular complex from the $\Delta G^{\ddagger}_{303}$ value for the unsubstituted complex Re(bpy)(CO)$_3$H.

carbon of CO_2 in the TS for the Re complexes.[19f,19g] In agreement with this hypothesis, an inverse kinetic isotope effect (KIE) of $k_H/k_D = 0.60 \pm 0.08$ is observed when the rate constants for CO_2 insertion into Re(bpy)$(CO)_3$H and Re(bpy)$(CO)_3$D are compared. Although inverse isotope effects are often observed in CO_2 insertion reactions because the strength of the C–H bond formed is greater than the strength of the M–H bond broken, this is a relatively large inverse isotope effect that is consistent with a late TS in which there is a stronger interaction between the hydride and the carbon of CO_2.[19f,19g]

Next, we systematically explored how the identity of the acceptor influences the kinetic hydricity of the Re hydride complexes. While it is expected that kinetic hydricity of a particular metal hydride will vary with the identity of the acceptor,[6b,6e,12,22] the present system provided a unique opportunity to explore how the Hammett slope and KIE change as a function of driving force effects and steric properties. Therefore, we explored hydride transfer from our Re hydrides to a range of hydride acceptors (Figures 4 and S15[23]). We studied hydride acceptors whose conjugate hydride donors have known thermodynamic hydricities in ACN, such as 1,3-dimethylpyridin-1-ium (^{Me}**Pic**$^+$),[12] 1,3-dimethyl-1H-benzo[d]imidazol-3-ium (^{Me}**BzIm**$^+$),[6c,12] 1,3-dimethyl-2-phenyl-1H-benzo[d]imidazol-3-ium (**Ph**^{Me}**BzIm**$^+$),[6c,24] 5-methylphenanthridin-5-ium (^{Me}**Ant**$^+$),[6c,8c] 10-methylacridin-10-ium (^{Me}**Acr**$^+$),[6c,14] 9-phenyl-10-methylacridin-10-ium (**Ph**^{Me}**Acr**$^+$),[6c,25] and the trityl cation (**Trit**$^+$).[6c,26] This provided a range of hydride acceptors whose conjugate hydride

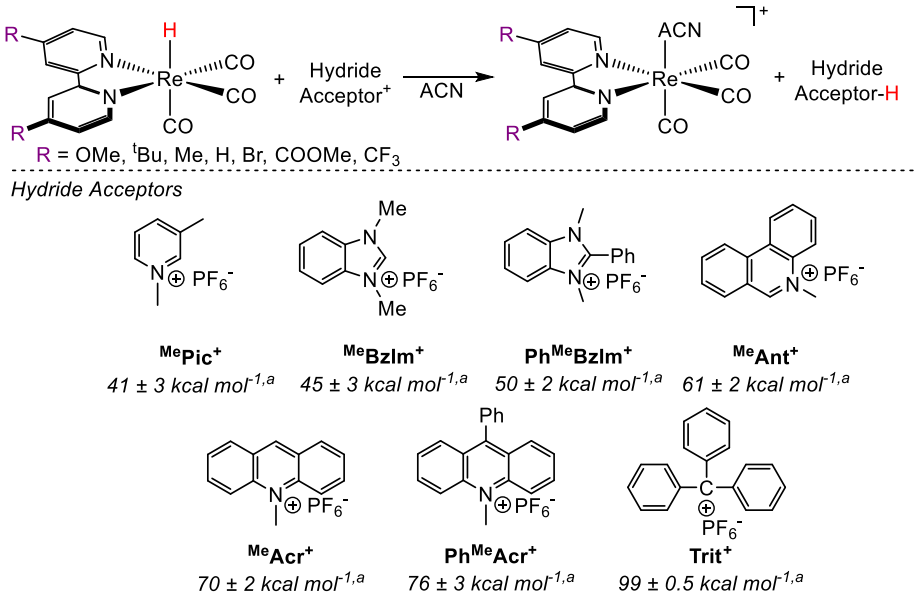

Figure 4: Hydride transfer reactions between our series of Re complexes and a variety of different hydride acceptors. [a]The value listed is the hydride affinity of the hydride acceptor (or the thermodynamic hydricity of the conjugate hydride donor) based on numbers previously reported in the literature.

Table 2: Activation parameters and kinetic isotope effects for hydride transfer from Re(bpy)(CO)$_3$H to different hydride acceptors in ACN at 30 °C.

Entry	Hydride Acceptor	Thermodynamic Hydricity kcal mol^{-1} [a]	$\Delta H^{\ddagger}$ kcal mol^{-1}	$\Delta S^{\ddagger}$ cal mol^{-1} k^{-1}	$\Delta G^{\ddagger}_{303}$ (kcal mol^{-1})	KIE (k_H/k_D)
1	^{Me}Pic$^+$	41 ± 3	15.8 ± 0.7	–16.6 ± 2.0	21.2 ± 0.3	0.38 ± 0.05
2	CO_2	44[b]	7.4 ± 0.9	–40.1 ± 2.8	19.6 ± 0.04	0.60 ± 0.08
3	^{Me}BzIm$^+$	45 ± 3	17.3 ± 0.7	–14.2 ± 2.0	22.0 ± 0.4	0.43 ± 0.06
4	Ph^{Me}BzIm$^+$	50 ± 2	17.3 ± 0.9	–19.6 ± 2.9	23.3 ± 0.07	0.45 ± 0.06
5	Ph^{Me}Acr$^+$	76 ± 3[c]	4.9 ± 0.4	–17.9 ± 1.3	10.1 ± 0.1	1.65 ± 0.23

[a]Thermodynamic hydricity of conjugate hydride donor of the chosen acceptor. [b]No error is included as 44 kcal mol^{-1} is an approximate hydride affinity for CO_2. [c]Uncertainty is estimated based on comparison with the error on thermodynamic hydricities measured using similar methods in the literature.

donors have thermodynamic hydricities between 41 and 99 kcal mol^{-1} to compare with hydride transfer to CO_2, whose conjugate hydride donor has a thermodynamic hydricity of 44 kcal mol^{-1}.[27]

Hydride transfer to the acceptors with the greatest hydride affinity — **^{Me}Ant$^+$**, **^{Me}Acr$^+$**, and **Trit$^+$** — is too fast for kinetics to be measured even using a stopped-flow instrument. Based on the instrument response factor, we estimate the rate constant for hydride transfer from Re(bpy)(CO)$_3$H to these substrates is >6.5 x 10^6 M^{-1}s^{-1}, assuming a bimolecular reaction. In contrast, the rates of hydride transfer to **Ph^{Me}Acr$^+$** could be measured using a stopped-flow instrument. Hydride transfer to **^{Me}Pic$^+$**, **^{Me}BzIm$^+$**, and **Ph^{Me}BzIm$^+$** is slower and we measured the rates for the majority of our Re hydrides by UV-Vis spectroscopic monitoring of shaken reaction solutions. However, for these acceptors the rates of hydride transfer from the electron deficient hydrides Re(^{R}bpy)(CO)$_3$H (R = COOMe and CF$_3$) were so slow that a significant amount of decomposition was observed and we were unable to obtain quantifiable data for these complexes. For the cationic N-heterocyclic acceptors, where we were able to measure the kinetics, the rate laws are k_1[Acceptor$^+$][Re(^{R}bpy)(CO)$_3$H], consistent with a bimolecular reaction (see Figures S20-23). Eyring analysis indicates that the entropies for hydride transfer to **^{Me}Pic$^+$**, **^{Me}BzIm$^+$**, **Ph^{Me}BzIm$^+$**, and **Ph^{Me}Acr$^+$** are similar (Table 2), consistent with the reactions proceeding via analogous TSs (*vide infra*). However, the entropies are much smaller than those associated with hydride transfer to CO_2. A possible explanation for this observation is that there is significantly more solvent ordering in the reaction with CO_2, as in this case two neutral molecules are forming a charged TS. In contrast, in hydride transfer to the cationic N-heterocyclic acceptors one of the starting materials is already charged, so a smaller amount of new solvent ordering required in the TS.[28]

To gain more information about how hydride transfer varies as the acceptor is changed, KIEs

(k_H/k_D) were measured for hydride transfer between Re(bpy)$(CO)_3$H or Re(bpy)$(CO)_3$D and ^{Me}**Pic**$^+$, ^{Me}**BzIm**$^+$, **Ph**^{Me}**BzIm**$^+$, and **Ph**^{Me}**Acr**$^+$ (Table 2). The KIEs increase as the thermodynamic driving force for the reaction increases. For example, the KIE for hydride transfer to ^{Me}**Pic**$^+$, which has the smallest driving force, is 0.38 ± 0.05, while the KIE for hydride transfer to **Ph**^{Me}**Acr**$^+$, which has the largest driving force, is 1.65 ± 0.05. For the hydride acceptors that display inverse kinetic isotope effects we propose that when the reactions involve a hydride donor and a hydride acceptor that are more closely matched energetically, the TS becomes more product-like. In the product, the C–H bond that is formed is stronger than the Re–H bond that is broken and as a result the magnitude of the inverse KIE is greater as the TS becomes more product-like. The change from inverse to normal KIE that is observed with **Ph**^{Me}**Acr**$^+$ is harder to interpret, although Bullock and co-workers observed a similar effect when they explored KIEs in hydride transfer reactions between metal hydrides with different thermodynamic hydricity and the trityl cation.[29] In their case, they proposed that when reactions have increased driving force, there is less involvement of force constants with isotopically sensitive modes in the TSs, and this could be also the case in our work. Overall, even though the exact reasons for the changes in KIE are unclear on a molecular level, our results demonstrate for the first time that KIEs for hydride transfer move in a relatively predictable fashion as the thermodynamic hydricity of the hydride acceptor is varied.

To probe if the effect of varying the electronic properties of the metal hydride influences the rate of hydride transfer to different hydride acceptors in a predictable fashion, we constructed Hammett plots for the transfer of a hydride from Re(^{R}bpy)$(CO)_3$H to ^{Me}**Pic**$^+$, ^{Me}**BzIm**$^+$, **Ph**^{Me}**BzIm**$^+$, and **Ph**^{Me}**Acr**$^+$ (Figure S28). All of the Hammett plots give negative slopes, indicating that more electron-donating substituents increase the rate of the reaction and suggesting that the reactions follow similar pathways. Given that thermodynamic hydricity is proposed to correlate with the Hammett parameter,[21] our data indicates that there is a generalizable correlation between the thermodynamic hydricity of the different Re hydrides and the rates at which they transfer a hydride, which extends across acceptors with a range in thermodynamic hydricity of at least 35 kcal mol^{-1}. Essentially, for any given hydride acceptor, the relative rate of hydride transfer from a Re hydride can be predicted based on the Hammett parameter of the Re hydride, which is likely related to their thermodynamic hydricity (*vide infra*).

Interestingly, when the slopes of the Hammett plot (ρ) for the different cationic N-heterocyclic

acceptors are compared to their hydride affinities, we observe an approximately linear decrease in ρ as the thermodynamic driving force increases (Figure 5). As the reaction becomes more thermodynamically favorable, the electronic differences between the bpy ligands become less important. We propose that in reactions in which there is less thermodynamic driving force, the TS is later and more product-like. If the TS is more product-like, the extent to which the Re–H bond is broken is greater and the Re center is more positively charged. The influence of the substituents on the bpy ligand would be expected to be greater when the Re center is more positively charged, explaining why reactions with less thermodynamic driving force have larger ρ values. This explanation is analogous with our proposal for the observed changes in KIEs.[30]

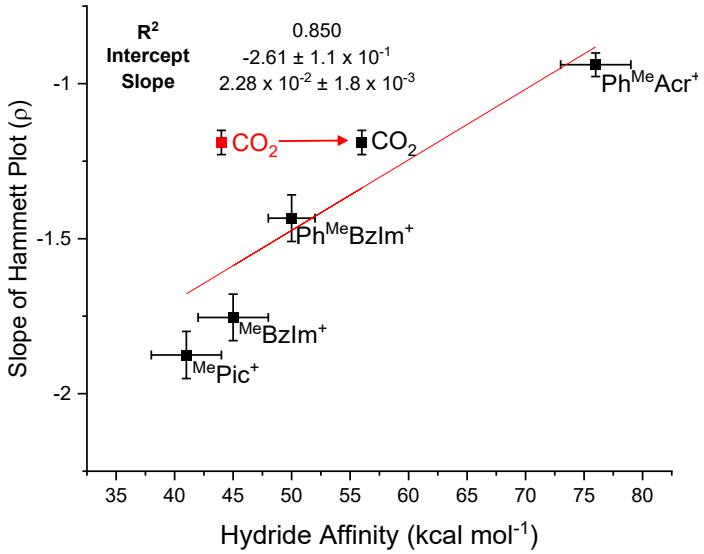

Figure 5: Correlation between the slope of the Hammett plot (ρ) and the hydride affinity of the acceptor. Effective thermodynamic hydride affinity is used for CO_2 (point shown in black). The uncorrected hydride affinity of CO_2 of 44 kcal mol^{-1} is shown in red, as this point is not included in the fit.

In our plot of ρ versus the hydride affinity of the acceptor, CO_2 is an outlier and has a much lower sensitivity to ligand electronic factors than would be expected based on the thermodynamic driving force for hydride transfer (red square in Figure 5). However, hydride transfer to CO_2 is the only reaction studied, where the product of hydride transfer, in this case the formate anion, binds to the metal center (Figure 3). Therefore, the metal containing product is a Re-formate, not a Re-ACN complex. Accordingly, when determining the thermodynamic driving force for this reaction, it is important to add the binding energy of formate to Re, so that an effective thermodynamic hydride affinity of CO_2 is calculated.[6e,31] For hydride transfer from $Re(bpy)(CO)_3H$ to CO_2, we estimate computationally that formate binding is approximately 12 kcal mol^{-1} more favorable than ACN

binding, and as a result the effective thermodynamic hydride affinity of CO_2 is 56.0 kcal mol^{-1} (see section SXIV and *vide infra*).[32] When this correction is made, CO_2 is no longer an outlier and gives a value of ρ, which enables an approximately linear fit for all data points (black markers in Figure 5). At this stage, the exact reasons why effective thermodynamic hydride affinity needs to be considered to obtain a linear fit are unclear, especially given that solvent binding is proposed to occur after the rate-determining step of hydride transfer (*vide infra*). Nevertheless, the empirical trend is clear, and this is the first time a relationship between the thermodynamic hydride affinity of the acceptor and the electronic sensitivity of the hydride donor has been derived.

Our experiments with different hydride acceptors enable us to compare how the absolute rate of hydride transfer from any one of our Re hydrides to the different hydride acceptors varies. We hypothesized that, as observed by Creutz *et al*., the rate of hydride transfer would become faster as the thermodynamic driving force for hydride transfer increased.[12] Qualitatively, our results with Re(bpy)(CO)$_3$H support this observation (Table 3 and see Tables S3-S8 for rates with other Re hydrides), as the rates of hydride transfer that are too fast to measure are observed for ^{Me}**Ant**$^+$, ^{Me}**Acr**$^+$, and **Trit**$^+$, which have some of the largest thermodynamic driving forces. Similarly, we can measure the rates of hydride transfer to ^{Me}**Pic**$^+$, ^{Me}**BzIm**$^+$, and **Ph**^{Me}**BzIm**$^+$, which have some of the lowest thermodynamic driving forces. However, more detailed analysis of the rates of hydride transfer from Re(bpy)(CO)$_3$H to ^{Me}**Pic**$^+$, ^{Me}**BzIm**$^+$, **Ph**^{Me}**BzIm**$^+$, and **Ph**^{Me}**Acr**$^+$ reveal a poor correlation with the thermodynamic driving force. In fact, the slowest rate of hydride transfer is observed to **Ph**^{Me}**BzIm**$^+$, which has a larger thermodynamic driving force than either ^{Me}**Pic**$^+$ or

Table 3: Experimental rates (k_1) for hydride transfer from Re(bpy)(CO)$_3$H to different hydride acceptors in ACN at 30 ˚C.

Entry	Hydride Acceptor	Thermodynamic Hydricity kcal mol^{-1},[a]	k_1 (M^{-1} s^{-1})[c]	Rate Relative to ^{Me}Pic$^+$
1	^{Me}Pic$^+$	41 ± 3	1.24 x 10^{-2}	-
2	^{Me}BzIm$^+$	45 ± 3	3.97 x 10^{-3}	0.33
3	Ph^{Me}BzIm$^+$	50 ± 2	3.68 x 10^{-4}	3.7 x 10^{-2}
4	CO_2	56[b]	4.28 x 10^{-2}	3.5
5	^{Me}Ant$^+$	61 ± 2[d]	> 6.5 x 10^6	NA
6	^{Me}Acr$^+$	70 ± 2	> 6.5 x 10^6	NA
7	Ph^{Me}Acr$^+$	76 ± 3[d]	2.01 x 10^5	1.6 x 10^7
8	Trit$^+$	99 ± 0.5	> 6.5 x 10^6	NA

[a]Thermodynamic hydricity of conjugate hydride donor of the chosen acceptor. [b]Effective thermodynamic hydride affinity including formate binding. No error is included as the initial value of 44 kcal mol^{-1} before the correction for formate binding is an approximate hydride affinity for CO_2. [c]A 10% error is associated with the rate. [d]Uncertainty is estimated based on comparison with the error on thermodynamic hydricities measured using similar methods in the literature.

^{Me}**BzIm**$^{+}$. Similarly, it is surprising that we can measure a rate for hydride transfer to **Ph**^{Me}**Acr**$^{+}$, when it is a significantly better hydride acceptor than ^{Me}**Ant**$^{+}$ or ^{Me}**Acr**$^{+}$. This data suggests that the thermodynamic hydricity of the acceptor is not the only factor that needs to be considered in understanding the rates of hydride transfer.

Steric Effects on Kinetic Hydricity

We hypothesized that steric factors may be causing the decrease in the relative rate of hydride transfer to **Ph**^{Me}**BzIm**$^{+}$ and **Ph**^{Me}**Acr**$^{+}$ compared to other acceptors. This would explain why hydride transfer to ^{Me}**Pic**$^{+}$ is faster than hydride transfer to either of the more sterically congested acceptors ^{Me}**BzIm**$^{+}$ or **Ph**^{Me}**BzIm**$^{+}$, despite the lower thermodynamic driving force.[33] To rigorously assess the influence of steric factors, we synthesized 1,3-R_2-1H-benzo[d]imidazol-3-ium cations (^{R}**BzIm**$^{+}$) (R = Me, Et, Pr, ^{i}Pr), which have similar thermodynamic hydride affinities ($\Delta\Delta G°_{H-}$ between the acceptors is 0.7 kcal mol^{-1}) but varied steric properties (see sections SXVI & SXVII). We then quantified the rate of hydride transfer from Re(^{OMe}bpy)(CO)$_3$H to the different acceptors (Figure 6). Consistent with our proposal, there is a difference of one order of magnitude in rate constant for hydride transfer between ^{Me}**BzIm**$^{+}$ and ^{Et}**BzIm**$^{+}$ and a staggering three orders of magnitude between ^{Me}**BzIm**$^{+}$ and ^{iPr}**BzIm**$^{+}$. These results suggest that the deviations we observe

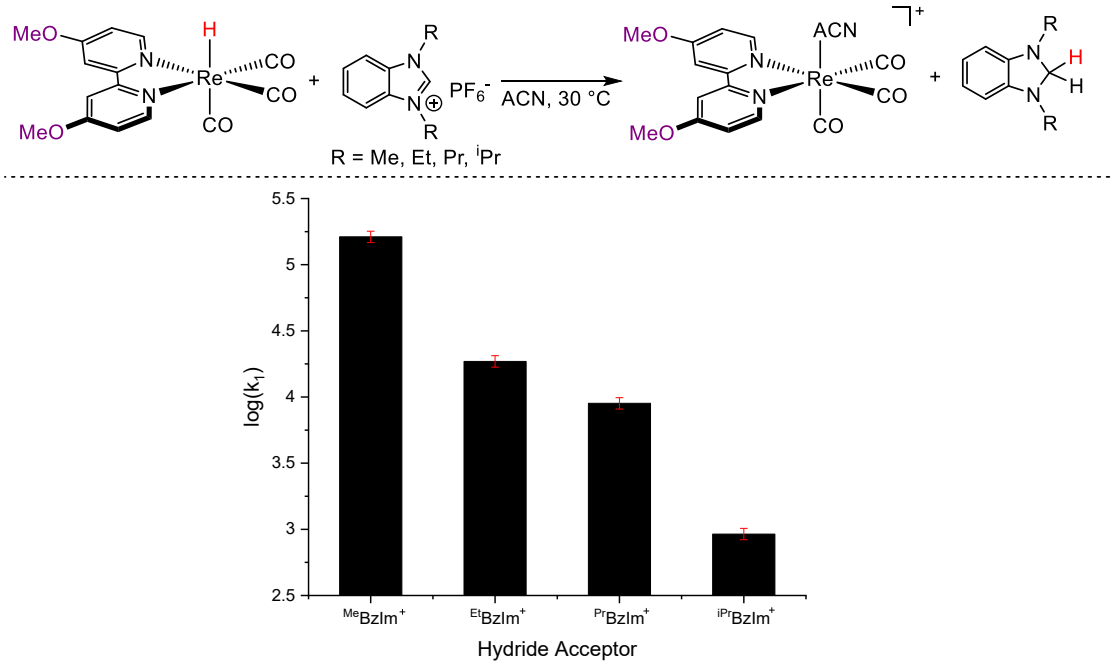

Figure 6: Rates of hydride transfer from Re(^{OMe}bpy)(CO)$_3$H to hydride acceptors with different steric properties but similar thermodynamic hydricities. Rates have units of μM^{-1} s^{-1} and have an error of ±10 %.

between the rate constant for hydride transfer (Table 3) and the thermodynamic driving force for the reaction with cationic N-heterocycles are related to steric factors.

Given that steric differences between hydride acceptors cause deviations in the relationship between the rate of hydride transfer and the thermodynamic driving force for the reaction, we hypothesized that a similar effect would be observed when the steric properties around the metal hydride were altered. To examine this, we synthesized Re(6,6'-dimethyl-2,2'-bipyridine)$(CO)_3H$ (Re($^{6\text{-Me}}$bpy)$(CO)_3H$) and measured its rates of hydride transfer to CO_2, ^{Me}**Pic**$^+$, ^{Me}**BzIm**$^+$, and **Ph^{Me}Acr**$^+$ (Table 4). In order, to place the measured rate constants for hydride transfer from Re($^{6\text{-Me}}$bpy)$(CO)_3H$ into the Hammett plots shown in Figures 3 and S28, a σ_p for the 6,6'-methyl substituents is required. This is problematic because *ortho* Hammett parameters do not exist. However, Kubiak *et al.* showed that there is a linear relationship between the electrochemical reduction potentials for complexes of the type Re(^{R}bpy)$(CO)_3Cl$ and their Hammett parameter.[34] Using this relationship, we estimate that Re($^{6\text{-Me}}$bpy)$(CO)_3H$ has a $\Sigma\sigma_p$ of –0.26 (see section SXVIII). Although this σ_p reflects both electronic and steric changes associated with the introduction of the 6,6'-methyl substituents, the steric impact is likely minimal because theoretical calculations show the geometrical parameters around the Re center in Re($^{6\text{-Me}}$bpy)$(CO)_3H$ are essentially the same as our other Re hydrides. Thus, the estimated $\Sigma\sigma_p$ primarily reflects the electronic properties of the complex.

Table 4: Predicted and measured rates for hydride transfer from Re($^{6\text{-Me}}$Bpy)$(CO)_3H$ to different hydride acceptors in ACN at 30 ˚C.

Entry	Acceptor	Thermodynamic Hydricity (kcal mol^{-1})[a]	Predicted k_1 Re($^{6\text{-Me}}$bpy)$(CO)_3H$ (M^{-1} s^{-1})[b]	Measured k_1 Re($^{6\text{-Me}}$bpy)$(CO)_3H$ (M^{-1} s^{-1})[c]	Rate Decrease
1	^{Me}Pic$^+$	41 ± 3	4.46 x 10^{-2}	4.01 x 10^{-3}	11
2	^{Me}BzIm$^+$	45 ± 3	2.14 x 10^{-2}	1.10 x 10^{-3}	20
3	CO_2	56[d]	8.50 x 10^{-2}	2.00 x 10^{-2}	4.3
4	Ph^{Me}Acr$^+$	68 ± 3[e]	4.00 x 10^5	9.33 x 10^4	4.3

[a]Thermodynamic hydricity of conjugate hydride donor of the chosen acceptor. [b]Value predicted from using Hammett plots in Figures 3 and S28 based on a Σ_p of -0.26 (see section SXVIII). [c]A 10% error is used for the k_1 value. [d]Effective thermodynamic hydride affinity including formate binding. No error is included as the initial value of 44 kcal mol^{-1} before the correction for formate binding is an approximate hydride affinity for CO_2. Uncertainty is estimated based on comparison with the error on thermodynamic hydricities measured using similar methods in the literature.

Table 4 shows the predicted rate of hydride transfer from Re($^{6\text{-Me}}$bpy)$(CO)_3H$ based only on its estimated $\Sigma\sigma_p$ and the linear equation fitting the Hammett plots for the 4-substituted bpy complexes (see Figures 3, S28, and S36). For all hydride acceptors, we observed experimental

rates that are slower for Re($^{6\text{-Me}}$bpy)(CO)$_3$H than: (i) those predicted based solely on the estimated $\Sigma\sigma_p$ value and (ii) those obtained for the analogous 4,4'-substituted bpy hydride, Re(^{Me}bpy)(CO)$_3$H. In general, the effect is more significant for hydride acceptors that are also sterically bulky, so hydride transfer to ^{Me}**BzIm**$^+$ is 20 times slower than the expected rate based solely on the $\Sigma\sigma_p$ value, while transfer to less bulky CO_2 is only 4 times slower. This is consistent with the decrease in rate being related to the 6,6'-methyl groups resulting in increased steric clash in the TS, which is supported by DFT calculations. However, **Ph^{Me}Acr**$^+$, which is one of the bulkiest hydride acceptors, is an exception to this trend and displays a rate that is only 4 times slower than the predicted value. It is possible that the steric factors associated with the metal hydride are comparatively less important in this case because there is a stronger thermodynamic driving force for the reaction, which means that there is a less pronounced interaction between the metal hydride and the acceptor in the TS. Taken together, our results show that steric factors are important in determining the rate of hydride transfer and that even small changes to either the hydride donor or acceptor can lead to substantial deviations from what is expected based on the thermodynamic driving force for a reaction.

Experimental and Computational Estimation of Thermodynamic Hydricity

To develop LFERs between kinetic and thermodynamic hydricity, we needed to obtain thermodynamic hydricities for our family of Re hydrides. Attempts to experimentally determine thermodynamic hydricity according to thermochemical cycles were unsuccessful (see sections SXXI-XXIII for details).[6b] However, the potential-pK_a method[27a] allowed us to estimate that the thermodynamic hydricity of Re(bpy)(CO)$_3$H is > 40 kcal mol^{-1} (see Section SXXIII). As traditional thermochemical methods did not yield a precise thermodynamic hydricity, we approximated a value using the known linear correlation between the first reduction potential of a metal solvato complex and the thermodynamic hydricity of its corresponding metal hydride developed by Kubiak *et al.*[6d] Using cyclic voltammetry, we determined the reduction potentials of Re(^{R}bpy)(CO)$_3$(ACN)$^+$ (R = OMe, Me, H) in ACN and then utilized the previously established relationships to estimate that the thermodynamic hydricities of Re(^{OMe}bpy)(CO)$_3$H, Re(^{Me}bpy)(CO)$_3$H, and Re(^{H}bpy)(CO)$_3$H are 42, 43, and 45 kcal mol^{-1}, respectively (see section SXXIV). The predicted hydricity for the unsubstituted complex Re(bpy)(CO)$_3$H agrees with our lower bound of 40 kcal mol^{-1} and is consistent within error with our hydride transfer reactions, as we observe hydride transfer to ^{Me}**Pic**$^+$, which has a hydride affinity of 41 ± 3 kcal mol^{-1}. Further,

the electrochemical data suggests that Re(^{OMe}bpy)(CO)$_3$H and Re(^{Me}bpy)(CO)$_3$H are more hydridic than the unsubstituted species, which is in line with our experimental kinetic data and the proposed correlation between Hammett parameter and thermodynamic hydricity.[21]

To more precisely determine the thermodynamic hydricity of our family of Re(^{R}bpy)(CO)$_3$H complexes, we turned to computational approaches and performed calculations using density functional theory (DFT) and wavefunction based methods (see section SXXV). Using the M06 functional[35] in conjunction with the def2-TZVPP basis set[36] and SMD continuum solvation model[37] for ACN, the thermodynamic hydricity of Re(bpy)(CO)$_3$H is estimated to be 41.1 ± 1.5 kcal mol^{-1} (Table 5). This value was obtained by taking the average of computed thermodynamic hydricities from isodesmic equilibrium exchange reactions between Re(bpy)(CO)$_3$H and five other transition metal hydrides that range in experimental hydricity from 36 to 62 kcal mol^{-1} and vary in charge (see Table S13).[6e] Several other popular density functionals (Table S43) and calculations at the DLPNO-CCSD(T)/def2-TZVPP level of theory[38] (Table S44) resulted in a similar value for the thermodynamic hydricity of Re(bpy)(CO)$_3$H. Overall, our calculated thermodynamic hydricity value for Re(bpy)(CO)$_3$H is in agreement with the value predicted experimentally using the first reduction potential.

We next calculated the relative thermodynamic hydricities of Re(^{R}bpy)(CO)$_3$H (R = OMe, ^{t}Bu, Me, Br, COOMe, CF$_3$) through isodesmic exchange reactions with Re(bpy)(CO)$_3$H using M06/def2-TZVPP, several other DFT methods, and DLPNO-CCSD(T)/def2-TZVPP (Tables 5 & S15-S25). In all cases, computed relative hydricities are similar, suggesting that the relative

Table 5: Computed relative and absolute thermodynamic hydricities of Re(^{R}bpy)(CO)$_3$H in ACN, determined through isodesmic exchange reactions with Re(bpy)(CO)$_3$H.

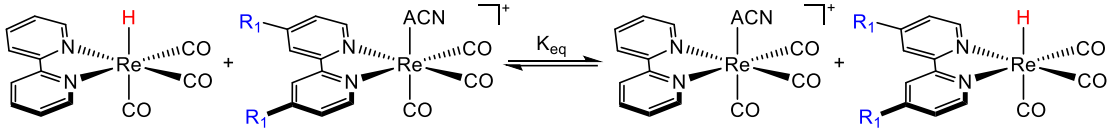

Re(^{R}bpy)(CO)$_3$H	Relative Thermodynamic Hydricity (kcal mol^{-1})	Computed Thermodynamic Hydricity (kcal mol^{-1})
Re(^{OMe}bpy)(CO)$_3$H	-1.2	39.9
Re(^{Me}bpy)(CO)$_3$H	-0.5	40.6
Re(^{tBu}bpy)(CO)$_3$H	-0.2	40.9
Re(bpy)(CO)$_3$H	0.0	41.1
Re(^{Br}bpy)(CO)$_3$H	1.2	42.3
Re(^{COOMe}bpy)(CO)$_3$H	2.4	43.5
Re(^{CF_3}bpy)(CO)$_3$H	1.7	42.8

[a]All computations were performed at the M06/def2-TZVPP level with SMD continuum solvation model for ACN.

thermodynamic hydricity is mostly invariant to the chosen level of theory. Hammett plots of relative thermodynamic hydricity versus $\Sigma\sigma_p$ for the different disubstituted bpy complexes displayed linear correlations, consistent with the proposed correlation between Hammett parameter and thermodynamic hydricity (Figures S49, S55-S56, & S63).[21] Using the computed thermodynamic hydricity of $Re(bpy)(CO)_3H$ and the relative values found for the substituted complexes, computed thermodynamic values were established for all of our complexes (Table 5). The overall trend in thermodynamic hydricity is that complexes containing more electron rich bpy ligands are more hydridic than compounds with less electron rich bpy ligands, which is consistent with a previous work on the thermodynamic hydricity of Ir complexes with electronically different bpy ligands.[21] The only counterintuitive result is that $Re(^{COOMe}bpy)(CO)_3H$ is less hydridic than $Re(^{CF_3}bpy)(CO)_3H$, but when computational errors are considered these values are quite similar.

Computational Modeling of Kinetic Hydricity

We calculated the kinetic hydricities of our family of $Re(^{R}bpy)(CO)_3H$ complexes with different acceptors, starting with hydride transfer to CO_2. The computed free energy profiles for CO_2 insertion into $Re(bpy)(CO)_3H$ (with and without explicit ACN solvent molecules) indicate outer-sphere hydride transfer to CO_2 to form **I** to be rate limiting, assuming facile rotation of the formate ligand in **I** to form **II** (Figure 7 and S47-S48). The TS (**TS-I**) for hydride transfer from Re to CO_2 features only an interaction between the hydride and the carbon atom of CO_2, with no interaction

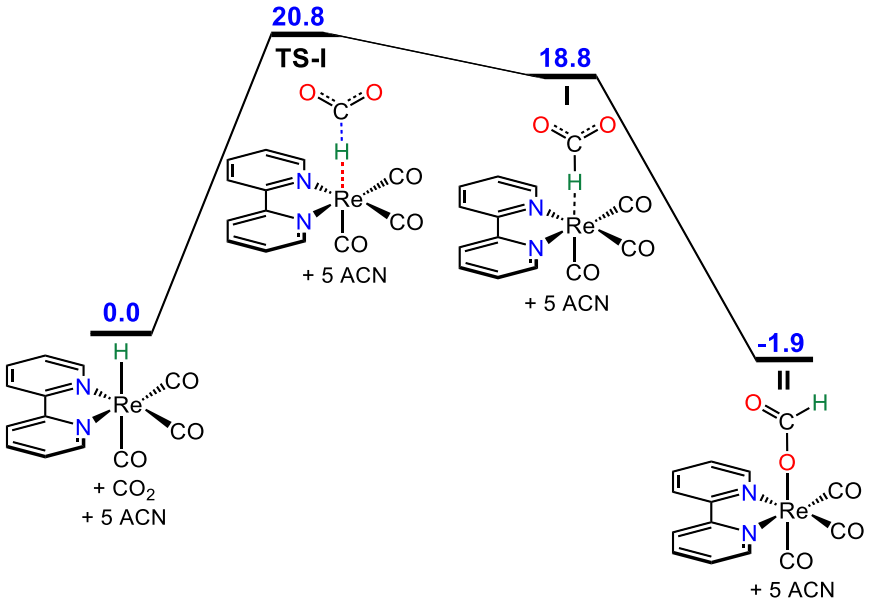

Figure 7. Computed free-energy profile (kcal mol^{-1}) for hydride addition to CO_2 to generate formate complex **II** with five explicit molecules of ACN included. For more information on the release of the formate ligand from Re in **II** to generate an ACN adduct, see Figure S47.

between Re and the oxygen atoms of CO_2. This type of outer-sphere TS is similar to calculated pathways for CO_2 insertion into a variety of other coordinatively saturated hydrides.[19a,39] It is, however, different compared with a previous calculation of CO_2 insertion into $Re(bpy)(CO)_3H$, which featured an inner-sphere pathway with both a Re–O and a C–H interaction in the initial TS.[40] Nevertheless, the previous result was obtained via geometry optimizations in vacuum. Consistent with our observation that formate remains coordinated to Re, the substitution of coordinated formate with a solvent ACN molecule was computed to be thermodynamically uphill (see Figures S47-S48).

When we consider CO_2 insertion into the full $Re(^{R}bpy)(CO)_3H$ series, we observe that the computed activation free energies ($\Delta G^{\ddagger}$) at the M06 level of theory (as well as other DFT methods and DLPNO-CCSD(T)/def2-TZVPP) exhibit strong correlations with the Hammett $\Sigma\sigma_p$ parameter (Figures S50, S61-S62, & S66), matching our experimental results. Further, at the M06 level of theory there is agreement between the computed and experimental activation energies and the computed activation energies are strongly correlated with the experimentally measured rate constants ($\ln(k_{expt})$) (Figure 8). This suggests that calculations can predict the rates of CO_2 insertion with complexes containing other substituents on the bpy ligand. We also investigated the geometric features, bond order properties, and partial atomic charges of the family of the Re hydrides, along with the TS associated with hydride transfer. No significant correlations were

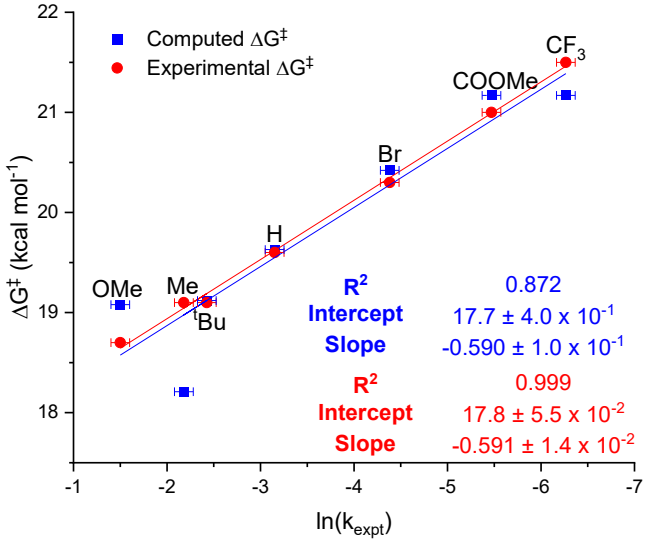

Figure 8. Plot of experimental activation free energies ($\Delta G^{\ddagger}_{expt}$, in red) and computed activation free energies ($\Delta G^{\ddagger}$, in blue) (kcal mol^{-1}) of $Re(^{R}bpy)(CO)_3H$ complexes versus the natural logarithm of relative experimental CO_2 insertion rates ($\ln(k_{expt})$) at M06/def2-TZVPP level of theory and 303 K.

observed except for the consistent differences in properties like C–H bond distance and bond order, and partial atomic charges of Re, H and C atoms in optimized TS structures between complexes supported by the most electron-donating (R = OMe) and most electron-withdrawing (R = CF_3) bpy ligands (Tables S26-S27). The TS is later and more product like for the CF_3 substituted ligand.

Next, we examined hydride transfer from Re(^{R}bpy)$(CO)_3$H to ^{Me}**Pic**$^+$, ^{Me}**BzIm**$^+$, **Ph**^{Me}**BzIm**$^+$, and **Ph**^{Me}**Acr**$^+$. These reactions involve a single TS in which the Re hydride bond is cleaved and the C–H bond is formed (Figure S81), consistent with concerted hydride transfer, as opposed to electron transfer (ET) followed by proton transfer (PT) or *vice versa*. After the hydride has transferred, the substrate presumably diffuses into solution, and solvent binds to the cationic metal center. The calculated activation energies for hydride transfer from Re(bpy)$(CO)_3$H follow a similar trend to the experimental activation energies (Table S28) with the barrier being lower for **Ph**^{Me}**Acr**$^+$ ($\Delta G^‡$ = 17.8 kcal mol^{-1}) than for ^{Me}**Pic**$^+$, ^{Me}**BzIm**$^+$, **Ph**^{Me}**BzIm**$^+$. However, the computed $\Delta G^‡$ of 17.8 kcal mol^{-1} is significantly higher than the experimentally measured $\Delta G^‡$ of 10.1 kcal mol^{-1} for **Ph**^{Me}**Acr**$^+$ and although our search for alternative conformers for the hydride transfer TS structure led to slightly lower activation free energies ($\Delta G^‡$ = 16.5 kcal mol^{-1}), the difference is still significant. We note that among the list of organic hydride acceptors investigated computationally, **Ph**^{Me}**Acr**$^+$ features the largest driving force and quantum tunneling effects might need to be considered for more accurate predictions.

The computed activation energy is higher for hydride transfer from Re(bpy)$(CO)_3$H to **Ph**^{Me}**BzIm**$^+$ ($\Delta G^‡$ = 21.5 kcal mol^{-1}) compared to that of ^{Me}**BzIm**$^+$ ($\Delta G^‡$ = 19.7 kcal mol^{-1}), in line with experimental trends and predicted steric effects. In contrast, the calculations cannot reproduce the observed experimental trend for ^{Me}**Pic**$^+$ ($\Delta G^‡$ = 22.9 kcal mol^{-1}), as it has a slightly higher calculated activation energy than ^{Me}**BzIm**$^+$, and **Ph**^{Me}**BzIm**$^+$. This minor discrepancy is unsurprising given the relatively small differences observed experimentally and the range of activation energies computed for different isomer products of ^{Me}**Pic**$^+$ ($\Delta G^‡$ = 19.7 and 20.6 kcal mol^{-1}). Inspection of geometric features, bond order properties, and partial atomic charges indicate relatively early TS structures for hydride transfer from Re(bpy)$(CO)_3$H to **Ph**^{Me}**Acr**$^+$ (Tables S39-S40) compared to ^{Me}**Pic**$^+$, ^{Me}**BzIm**$^+$, **Ph**^{Me}**BzIm**$^+$, as we hypothesized from our experimental trends. However, the computed properties are indistinguishable when comparing ^{Me}**Pic**$^+$, ^{Me}**BzIm**$^+$, and **Ph**^{Me}**BzIm**$^+$, most likely due to the similarities in the thermodynamic driving force for hydride

transfer, which mean that there are not large changes in the TS structure (Tables S29-S36). Similarly, when considering hydride transfer for the full series of Re(^{R}bpy)(CO)$_3$H complexes to ^{Me}**Pic**$^+$, ^{Me}**BzIm**$^+$, **Ph**^{Me}**BzIm**$^+$, and **Ph**^{Me}**Acr**$^+$, the only notable differences are observed between the most thermodynamically different complexes featuring either OMe or CF_3 substituents on the bpy. Specifically, the TS is always later for the CF_3 substituted complex.

The ability of the calculations to match experimental trends is further highlighted by the computed activation energies for hydride transfer from Re(bpy)(CO)$_3$H to the sterically diverse ^{R}**BzIm**$^+$ (R = Me, Et, Pr, and ^{i}Pr) series. The calculated activation energies are 19.7, 20.3, 21.4 and 23.0 kcal mol^{-1} respectively for R = Me, Et, Pr and ^{i}Pr (span from lowest to highest barrier is 3.3 kcal mol^{-1}, Table S42), consistent with the large steric effect observed experimentally. We also investigated hydride transfer from Re(^{CF_3}bpy)(CO)$_3$H and Re(^{OMe}bpy)(CO)$_3$H to the ^{R}**BzIm**$^+$ (R = Me, Et, Pr, and ^{i}Pr) series. The differences in computed activation energies for the sterically varied substrates were higher for Re(^{CF_3}bpy)(CO)$_3$H ($\Delta G^{\ddagger}$ = 20.6 (Me), 21.4 (Et), 23.2 (Pr), and 25.1 (^{i}Pr) kcal mol^{-1}; overall span is 4.5 kcal mol^{-1}) and smaller for Re(^{OMe}bpy)(CO)$_3$H ($\Delta G^{\ddagger}$ = 18.7 (Me), 18.6 (Et), 19.0 (Pr), and 19.1 (^{i}Pr) kcal mol^{-1}; overall span is 0.4 kcal mol^{-1}). This suggests that the extent of steric effects may be related to the thermodynamic hydricity of the hydride donor and that when there is a less hydridic donor and therefore a smaller thermodynamic driving force for the reaction, steric factors are magnified, presumably because there are more steric clashes in a later TS. Our experimental studies using Re($^{6\text{-}Me}$bpy)(CO)$_3$H also suggest that the effect of steric factors on rate may be related to the thermodynamic driving force for the reaction. Overall, our kinetic calculations show that: (i) hydride transfer is rate-determining and concerted in the reactions we are studying; (ii) as the reaction becomes more thermodynamically favorable either by varying the hydride donor or acceptor, the TS becomes earlier; and (iii) steric effects are large but influenced by the overall reaction thermodynamics.

Linear Free Energy Relationships and Marcus Analysis

Using the computed thermodynamic hydricities for Re(^{R}bpy)(CO)$_3$H (R = OMe, ^{t}Bu, Me, H, Br, COOMe, CF_3), we examined the relationship between thermodynamic hydricity and the experimental rates of CO_2 insertion. Figure 9A plots the natural logarithm of the rate constant for CO_2 insertion versus thermodynamic hydricity and shows that more hydridic complexes give faster rates of insertion. The kinetic hydricity is related to the activation energy of a specific hydride

transfer reaction from Re to CO_2, while the thermodynamic hydricity represents the dissociation of H^- and does not involve CO_2. Thus, the correlation is significant because it relates a *fundamental thermodynamic property* of the metal complex to the kinetics of a *specific reaction*. However, although this plot represents an elegant demonstration of a LFER between kinetic and thermodynamic hydricity, further analysis is difficult because the units of the values on the x and y axis are not the same. Therefore, in Figure 9B, we generated a classical Brønsted plot of $\ln(K_{eq})$ (where K_{eq} is the equilibrium constant for the hydride transfer reaction derived from the calculated thermodynamic hydricity of the transition metal hydride and the experimental value for the hydride acceptor) against $\ln(k_1)$ (where k_1 is the rate constant for hydride transfer at 303 K) for the hydride transfer reaction.[41] This is analogous to what has been plotted in the literature for organic hydride transfer reactions[8a-f]. Our LFER has a slope (Brønsted α) of 0.790 ± 0.02, which is within the range observed for reactions between organic hydride donors and acceptors. The α value is consistent with hydride transfer to CO_2 involving a *concerted* hydride transfer TS.[8d,8i] Further support for the concerted reaction comes from the Eyring analyses (*vide supra*), which gave rise to activation parameters in the expected range for a concerted process. This is because hydride transfer reactions that proceed via stepwise ET-PT-ET pathways have been reported to exhibit inverse temperature

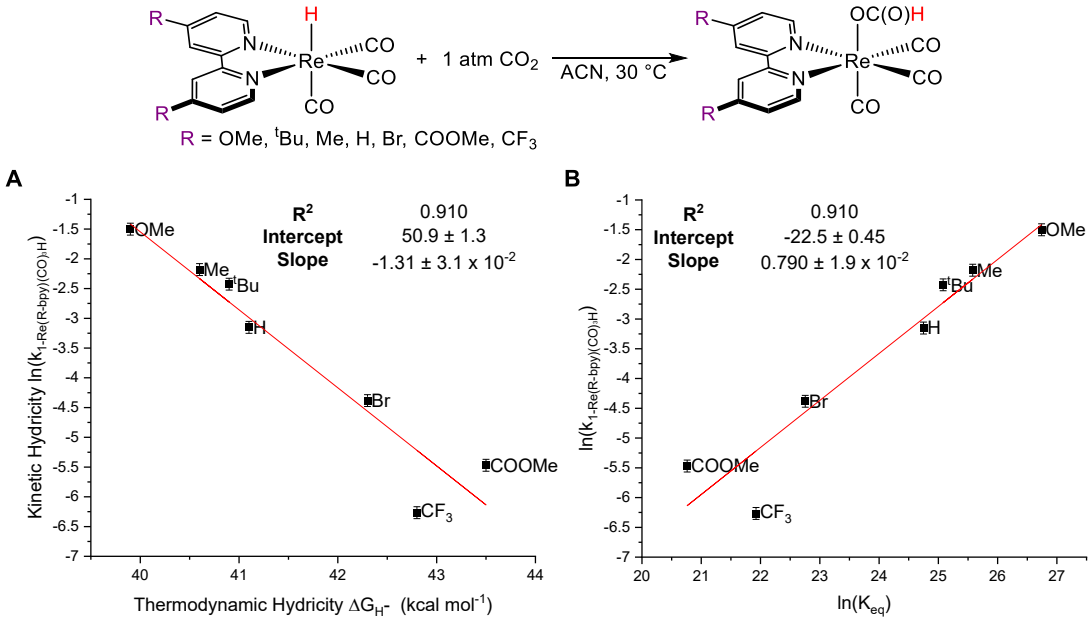

Figure 9: LFERs for CO_2 insertion into $Re(^{R}bpy)(CO)_3H$. (**A**) LFER comparing thermodynamic hydricity and the ln of the rate of hydride transfer, or kinetic hydricity. (**B**) Brønsted plot comparing thermodynamic hydricity and the ln of the rate constant. The slope of the plot (α) is 0.790. This plot uses the effective hydride affinity of CO_2, including formate binding to $Re(bpy)(CO)_3(ACN)^+$ (56 kcal mol^{-1}) to calculate K_{eq} ($\ln(K_{eq})=-\Delta G/RT$), but the slope is the same if absolute hydricity (44 kcal mol^{-1}) is used. Reaction conditions: [$Re(^{R}bpy)(CO)_3H$]: ~0.3 mM, [CO_2]: 0.26 M, ACN, 30 °C.

dependence (and thus negative $\Delta H^{\ddagger}$ values), which is not observed here.[42] Finally, in the case of CO_2 insertion, our extensive experimental data also enables us to plot the activation energies ($\Delta G^{\ddagger}$) for CO_2 insertion into Re(^{R}bpy)$(CO)_3H$ against the computed thermodynamic hydricity and as expected this shows a linear relationship, with a slope that is essentially the same as the plot of kinetic versus thermodynamic hydricity in Figure 9A (see Figure S83). Importantly, when we plot activation energies from theory against the computed thermodynamic hydricities, we see similar trends, suggesting that in the future, theory can be used to develop robust LFERs.

Linear correlations between thermodynamic and kinetic hydricity are also observed in the Brønsted plots for the reactions of our family of Re hydrides with ^{Me}**Pic**$^+$, ^{Me}**BzIm**$^+$, **Ph**^{Me}**BzIm**$^+$, and **Ph**^{Me}**Acr**$^+$ (Figure S82). In each plot, the slope is positive, indicating more rapid hydride transfer with more hydridic metal hydrides. However, the magnitude of the slope (α) changes by approximately a factor of two across the series of hydride donors/acceptors. Further, the value of α for each specific hydride transfer reaction has an approximately linear relationship with the hydride affinity of the chosen acceptor (Figure 10). It is notable that the slope of the LFER for hydride transfer to CO_2 fits well with the full data set *only* when we also consider *effective hydride affinity*. It could easily be assumed that only the H^- transfer would be related to the barrier of hydride transfer, but Figure 10 shows that the binding of formate to the Re center must be accounted for in analyzing LFERs. This has implications for catalysis, as it implies that the binding of a substrate after hydride transfer can impact the expected rate. In future work, we will investigate

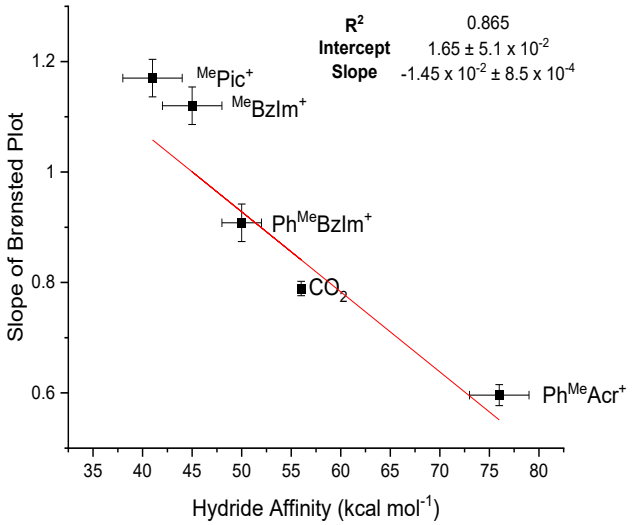

Figure 10: Correlation between the slope of Brønsted plots and thermodynamic hydricity of the conjugate hydride acceptor. Effective thermodynamic hydride affinity is used for CO_2, which is calculated by estimating the binding energy of formate to $[Re(bpy)(CO)_3(ACN)]^+$.

the exact reasons why *effective hydride affinity* needs to be considered for CO_2 insertion and potentially other substrates where binding occurs after H^- transfer.

The results in Figure 10 indicate that as the hydride affinity of the acceptor increases, and the overall driving force for hydride transfer increases, the activation barrier becomes *less sensitive* to changes in the thermodynamic hydricity of the hydride donor. In other words, changes in the thermodynamic hydricity of $Re(^{R}bpy)(CO)_3H$ have a much smaller influence on the rate of hydride transfer when there is more considerable thermodynamic driving force for the reaction (*i.e.,* when $\mathbf{Ph^{Me}Acr^+}$ is a hydride acceptor). In contrast, if there is a low thermodynamic driving force for the reaction, such as hydride transfer to $\mathbf{^{Me}Pic^+}$, then differences in the thermodynamic hydricity of $Re(^{R}bpy)(CO)_3H$ have a much larger influence on the rate of hydride transfer. Thus, our data suggests that optimizing the hydricity of a metal hydride complex is more critical when the thermodynamic driving force for the reaction is smaller. One important example that fulfills this criterion is catalytic reactions, where efficient catalysts have free energies of reaction for each step that are close to zero. Consequently, our analysis suggests that thermodynamic hydricity tuning is likely to have particularly large impacts on the rates of hydride transfer steps in catalysis. We also expect our finding (that the rates of hydride transfer reactions, which are more thermodynamically favorable, are less sensitive to changes in the thermodynamic hydricity) will be relevant to reactions involving organohydrides, where this trend has yet to be observed.

The linear correlation between α and the hydride affinity of the chosen acceptor suggests a similar hydride transfer mechanism across the different acceptors, where the TS becomes more product-like at lower driving forces. Accordingly, it may be possible to use Marcus theory to model single-step hydride transfer reactions from transition metal hydrides, as has been conducted for organic hydrides.[8a-f,9] To probe this hypothesis, we combined all the data sets used in the Brønsted plots into a single plot of $\ln(K_{eq})$ against $\ln(k_1)$ for hydride transfer to all of our acceptors (Figure 11). While the expected trend of increasing k_1 values with increasing driving force (larger K_{eq} values) is observed within each series where the Re complex is varied, and more broadly for three of the series where the acceptor is varied, a Marcus expression would clearly not fit all of the data. This is likely because of the different steric properties of our hydride acceptors and indicates that it is not possible to make general conclusions about the rates of hydride transfer to an acceptor based on thermodynamic considerations and/or Marcus theory alone, unless the acceptors have similar

steric profiles. Further, we have not included any data from the *ortho*-bpy substituted complex Re($^{6\text{-Me}}$bpy)(CO)$_3$H in Figure 11, because the rates of hydride transfer from this species are significantly slower than what would be expected based on its computed thermodynamic hydricity (42.2 kcal mol^{-1}). This implies that the steric properties of a metal complex can be used to independently tune the rates of hydride transfer, without changing the driving force. A potential application of this result is related to promoting selectivity in catalytic reactions, where a certain driving force may be needed for a substrate to accept a hydride, but by tuning the steric properties it could be possible to slow the donation of the hydride to a competing substrate with greater steric bulk.

To more rigorously assess our hypothesis that Marcus theory can be used to model reactions involving hydride acceptors with similar steric properties, we fit the data for hydride transfer to **Ph^{Me}BzIm$^+$** and **Ph^{Me}Acr$^+$**, which have similar steric profiles, using Eq 1 derived from Marcus theory as utilized by Kreevoy[8c] (see section SXXVIII):

$$\ln k_1 = \ln\left(\frac{k_B T}{h}\right) - \left(\frac{W^r}{RT}\right) - \left(\frac{\lambda}{4RT}\right) + \left(\frac{\ln K_{eq}}{2}\right) - \left(\frac{RT(\ln K_{eq})^2}{4\lambda}\right) \qquad (Eq\ 1)$$

where: k_1 is the observed rate constant for hydride transfer, k_B is the Boltzmann constant, T is temperature, h is Planck's constant, W^r is the standard free energy of formation of the precursor

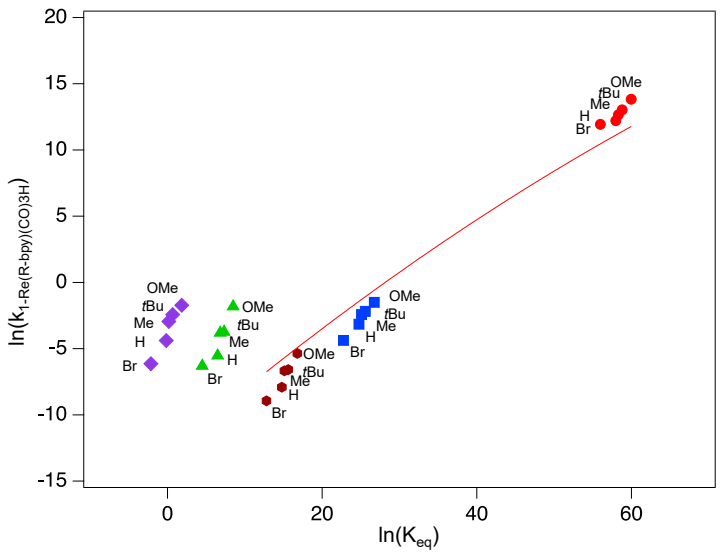

Figure 11: Brønsted plot comparing thermodynamic hydricity and the ln of the rate constant for hydride transfer from Re(^{R}bpy)(CO)$_3$H to CO_2 (blue squares), **^{Me}Pic$^+$** (purple diamonds), **^{Me}BzIm$^+$** (green triangles), **Ph^{Me}BzIm$^+$** (maroon hexagons), and **Ph^{Me}Acr$^+$** (red circles). The solid red line is the least-squares fit to the Marcus expression of Eq 1 only for the data sets involving hydride transfer to **Ph^{Me}BzIm$^+$**, and **Ph^{Me}Acr$^+$** with W^r = 0.0 kcal mol^{-1}. A λ value of 100.3 kcal mol^{-1} is estimated.

configuration from the reactants estimated as the electrostatic work term, R is the gas constant, λ is the reorganization energy, K_{eq} is the equilibrium constant for hydride transfer. Based on a Coulombic model, we estimated W^r as 0 kcal mol^{-1} (see SI) and in this case, the red fitted line in Figure 11 gives good agreement with our experimental data and estimates a reorganization energy (λ) value of approximately 100 kcal mol^{-1}. This is similar to what has been observed for organic hydride transfer reactions[8c] but needs to be considered with caution because λ is highly sensitive to changes in W^r (see Figure S85). Further, using a W^r value of 0, we fitted data for ln(K_{eq}) against ln(k_1) for hydride transfer from Re(^{R}bpy)(CO)$_3$H to each individual hydride acceptor using Eq 1 (see Figures S86-S95). Relatively good fits are observed with λ values all in the range of 75-115 kcal mol^{-1}. This supports the proposal that when the steric properties of the metal hydride and organic acceptor are similar, Marcus theory can be used to model hydride transfer reactions. However, a prediction from Glusac *et al.*, derived from metal hydride and organohydride self-exchange kinetic data, is that λ values involving metal hydride complexes may be smaller than those involving purely organic hydrides.[9a] This highlights that kinetic studies of "cross reactions" of metal hydrides and organic acceptors with similar steric properties and spanning a large range in driving force are needed to provide conclusive insight. In future work, we will pursue this goal and quantify the reorganization energies, especially in comparison to hydride transfer reactions between organic systems. Nevertheless, our preliminary work demonstrates that with some caveats the types of Marcus analysis that have been performed for purely organic hydride transfer reactions are likely to be applicable to reactions that involve hydride transfer from transition metal hydrides.

Conclusions

In this work, we have measured the second-order rate constants of hydride transfer (kinetic hydricity) from a series of structurally similar but electronically distinct Re hydrides to a diverse set of hydride acceptors. Using primarily computational methods, verified with some experimental measurements, we determined the thermodynamic hydricity of our Re hydrides, which enabled us to develop some of the most comprehensive LFERs reported to date involving thermodynamic and kinetic hydricity of transition metal complexes. In general, we observe that as the thermodynamic driving force for hydride transfer increases, the rate of hydride transfer also increases. This is true for reactions in which the thermodynamic driving force for hydride transfer varies by up to 35 kcal mol^{-1} and appears to be independent of the exact structure of the hydride acceptor. Further,

reactions for which there is more thermodynamic driving force are less sensitive to changes in the electronic properties of the metal hydride, presumably because there is less build-up of charge in the earlier TS. However, even slight perturbations in the steric properties of the Re hydride or the hydride acceptor result in large deviations in the predicted rate of hydride transfer based on thermodynamic driving forces. In fact, the correlations between kinetic and thermodynamic hydricity for our transition metal complexes breakdown dramatically when steric factors are introduced. We expect that steric factors can also cause deviations from the LFERs observed in hydride transfer reactions involving purely organic systems, but this has not been studied to date.[8a-f] The observation that steric factors are important is significant to catalysis, as it indicates that when a substrate or catalyst is changed, the steric properties of the new substrate or catalyst, as well as the change in thermodynamic driving force, need to be considered when trying to predict reaction kinetics. In fact, it may be possible to use small changes in steric properties to influence selectivity in catalysis, as our results suggest that steric effects are non-linear. Finally, our results suggest that it in some cases it will be possible to use Marcus theory to analyze hydride transfer from transition metal hydrides and serve as a powerful predictive tool to control the rates of hydride transfer, which will be useful for the development of new and more active metal hydride catalysts.

Acknowledgements

NH acknowledges support from the National Science Foundation through Grant CHE-1953708 and the Yale Center for Natural Carbon Capture. The work at Brookhaven National Laboratory (M.Z.E) was carried out under contract DE-SC0012704 with the U.S. Department of Energy, Office of Science, Office of Basic Energy Sciences, and utilized computational resources at the Center for Functional Nanomaterials, which is a U.S. Department of Energy Office of Science Facility, and the Scientific Data and Computing Center, a component of the Computational Science Initiative, at Brookhaven National Laboratory under Contract No. DE-SC0012704. Aspects of the work on thermodynamic hydricity were supported by the U.S. Department of Energy, Office of Science, Office of Basic Energy Sciences, under Award No. DE-SC0014255 (A.M.S. and A.J.M.M.). Q.J.B. acknowledges support from the NSF Graduate Research Fellowship Program (DGE-1650116) and the UNC Dissertation Completion Fellowship Program. We thank Professor James Mayer for valuable discussions.

Additional information

Additional information about selected experiments, characterizing data, NMR spectra, computational information and other details are available via the Internet at https://pubs.acs.org/.

Competing Financial Interests

The authors declare no competing financial interests.

References

1. For examples related to the hydrogenation and dehydrogenation of CO_2 to formic acid or methanol, see: (a) Cokoja, M.; Bruckmeier, C.; Rieger, B.; Herrmann, W. A.; Kühn, F. E. Transformation of Carbon Dioxide with Homogeneous Transition-Metal Catalysts: A Molecular Solution to a Global Challenge? *Angew. Chem. Int. Ed.* **2011**, *50*, 8510-8537; (b) Goeppert, A.; Czaun, M.; Jones, J.-P.; Surya Prakash, G. K.; Olah, G. A. Recycling of Carbon Dioxide to Methanol and Derived Products – Closing the Loop. *Chem. Soc. Rev.* **2014**, *43*, 7995-8048; (c) Li, Y.-N.; Ma, R.; He, L.-N.; Diao, Z.-F. Homogeneous Hydrogenation of Carbon Dioxide to Methanol. *Catal. Sci. Technol.* **2014**, *4*, 1498-1512; (d) Wang, W.-H.; Himeda, Y.; Muckerman, J. T.; Manbeck, G. F.; Fujita, E. CO_2 Hydrogenation to Formate and Methanol as an Alternative to Photo- and Electrochemical CO_2 Reduction. *Chem. Rev.* **2015**, *115*, 12936-12973; (e) Klankermayer, J.; Wesselbaum, S.; Beydoun, K.; Leitner, W. Selective Catalytic Synthesis Using the Combination of Carbon Dioxide and Hydrogen: Catalytic Chess at the Interface of Energy and Chemistry. *Angew. Chem. Int. Ed.* **2016**, *55*, 7296-7343; (f) Bernskoetter, W. H.; Hazari, N. Reversible Hydrogenation of Carbon Dioxide to Formic Acid and Methanol: Lewis Acid Enhancement of Base Metal Catalysts. *Acc. Chem. Res.* **2017**, *50*, 1049-1058; (g) Sordakis, K.; Tang, C.; Vogt, L. K.; Junge, H.; Dyson, P. J.; Beller, M.; Laurenczy, G. Homogeneous Catalysis for Sustainable Hydrogen Storage in Formic Acid and Alcohols. *Chem. Rev.* **2018**, *118*, 372-433.

2. For examples related to the hydrogenation of unsaturated substrates, see: (a) Bäckvall, J.-E. Transition Metal Hydrides as Active Intermediates in Hydrogen Transfer Reactions. *J. Organomet. Chem.* **2002**, *652*, 105-111; (b) Blaser, H.-U.; Malan, C.; Pugin, B.; Spindler, F.; Steiner, H.; Studer, M. Selective Hydrogenation for Fine Chemicals: Recent Trends and New Developments. *Adv. Synth. Catal.* **2003**, *345*, 103-151; (c) Clapham, S. E.; Hadzovic, A.; Morris, R. H. Mechanisms of the H_2-Hydrogenation and Transfer Hydrogenation of Polar Bonds Catalyzed by Ruthenium Hydride Complexes. *Coord. Chem. Rev.* **2004**, *248*, 2201-2237; (d) Johnson, N. B.; Lennon, I. C.; Moran, P. H.; Ramsden, J. A. Industrial-Scale Synthesis and Applications of Asymmetric Hydrogenation Catalysts. *Acc. Chem. Res.* **2007**, *40*, 1291-1299; (e) Wang, D.; Astruc, D. The Golden Age of Transfer Hydrogenation. *Chem. Rev.* **2015**, *115*, 6621-6686; (f) Seo, C. S. G.; Morris, R. H. Catalytic Homogeneous Asymmetric Hydrogenation: Successes and Opportunities. *Organometallics* **2019**, *38*, 47-65; (g) Baidilov, D.; Hayrapetyan, D.; Khalimon, A. Y. Recent Advances in Homogeneous Base-Metal-Catalyzed Transfer Hydrogenation Reactions. *Tetrahedron* **2021**, *98*, 132435.

3. For examples related to alkene isomerization, see: (a) Hilt, G. Double Bond Isomerisation and Migration—New Playgrounds for Transition Metal-Catalysis. *ChemCatChem* **2014**, *6*, 2484-2485; (b) Larionov, E.; Li, H.; Mazet, C. Well-Defined Transition Metal Hydrides in Catalytic Isomerizations. *Chem. Commun.* **2014**, *50*, 9816-9826; (c) Hassam, M.; Taher, A.; Arnott, G. E.; Green, I. R.; van Otterlo, W. A. L. Isomerization of Allylbenzenes. *Chem. Rev.* **2015**, *115*, 5462-5569; (d) Vasseur, A.; Bruffaerts, J.; Marek, I. Remote Functionalization Through Alkene Isomerization. *Nature Chem.* **2016**, *8*, 209-219; (e) Massad, I.; Marek, I. Alkene Isomerization through Allylmetals as a Strategic Tool in Stereoselective Synthesis. *ACS Catal.* **2020**, *10*, 5793-5804; (f) Fiorito, D.; Scaringi, S.; Mazet, C. Transition Metal-Catalyzed Alkene Isomerization as an Enabling Technology in Tandem, Sequential and Domino Processes. *Chem. Soc. Rev.* **2021**, *50*, 1391-1406.

4. For examples related to hydroformylation, see: (a) Franke, R.; Selent, D.; Börner, A. Applied Hydroformylation. *Chem. Rev.* **2012**, *112*, 5675-5732; (b) Wu, X.-F.; Fang, X.; Wu, L.; Jackstell, R.; Neumann, H.; Beller, M. Transition-Metal-Catalyzed Carbonylation Reactions of Olefins and Alkynes: A Personal Account. *Acc. Chem. Res.* **2014**, *47*, 1041-1053; (c) Clarke, M. L. Hydroformylation. Fundamentals, Processes, and Applications in Organic Synthesis. By Armin Börner and Robert Franke. *Angew. Chem. Int. Ed.* **2016**, *55*, 13377-13377; (d) Nurttila, S. S.; Linnebank, P. R.; Krachko, T.; Reek, J. N. H. Supramolecular Approaches To Control Activity and Selectivity in Hydroformylation Catalysis. *ACS Catal.* **2018**, *8*, 3469-3488; (e) Chakrabortty, S.; Almasalma, A. A.; de Vries, J. G. Recent Developments in Asymmetric Hydroformylation. *Catal. Sci. Technol.* **2021**, *11*, 5388-5411; (f) Rodrigues, F. M. S.; Carrilho, R. M. B.; Pereira, M. M. Reusable Catalysts for Hydroformylation-Based Reactions. *Eur. J. Inorg. Chem.* **2021**, *2021*, 2294-2324.

5. For examples related to hydrosilylation, see: (a) Nakajima, Y.; Shimada, S. Hydrosilylation Reaction of Olefins: Recent Advances and Perspectives. *RSC Adv.* **2015**, *5*, 20603-20616; (b) Du, X.; Huang, Z. Advances in Base-Metal-Catalyzed Alkene Hydrosilylation. *ACS Catal.* **2017**, *7*, 1227-1243; (c) Obligacion, J. V.; Chirik, P. J. Earth-Abundant Transition Metal Catalysts for Alkene Hydrosilylation and Hydroboration. *Nature Rev. Chem.* **2018**, *2*, 15-34; (d) de Almeida, L. D.; Wang, H.; Junge, K.; Cui, X.; Beller, M. Recent Advances in Catalytic Hydrosilylations: Developments Beyond Traditional Platinum Catalysts. *Angew. Chem. Int. Ed.* **2021**, *60*, 550-565.
6. (a) McSkimming, A.; Colbran, S. B. The Coordination Chemistry of Organo-Hydride Donors: New Prospects for Efficient Multi-Electron Reduction. *Chem. Soc. Rev.* **2013**, *42*, 5439-5488; (b) Wiedner, E. S.; Chambers, M. B.; Pitman, C. L.; Bullock, R. M.; Miller, A. J. M.; Appel, A. M. Thermodynamic Hydricity of Transition Metal Hydrides. *Chem. Rev.* **2016**, *116*, 8655-8692; (c) Ilic, S.; Alherz, A.; Musgrave, C. B.; Glusac, K. D. Thermodynamic and Kinetic Hydricities of Metal-Free Hydrides. *Chem. Soc. Rev.* **2018**, *47*, 2809-2836; (d) Waldie, K. M.; Ostericher, A. L.; Reineke, M. H.; Sasayama, A. F.; Kubiak, C. P. Hydricity of Transition-Metal Hydrides: Thermodynamic Considerations for CO_2 Reduction. *ACS Catal.* **2018**, *8*, 1313-1324; (e) Brereton, K. R.; Smith, N. E.; Hazari, N.; Miller, A. J. M. Thermodynamic and Kinetic Hydricity of Transition Metal Hydrides. *Chem. Soc. Rev.* **2020**, *49*, 7929-7948.
7. (a) Mochida, I.; Yoneda, Y. Linear Free Energy Relationships in Heterogeneous Catalysis: I. Dealkylation of Alkylbenzenes on Cracking Catalysts. *J. Catal.* **1967**, *7*, 386-392; (b) Bjelic, S.; Åqvist, J. Catalysis and Linear Free Energy Relationships in Aspartic Proteases. *Biochemistry* **2006**, *45*, 7709-7723; (c) Miller, J. J.; Sigman, M. S. Quantitatively Correlating the Effect of Ligand-Substituent Size in Asymmetric Catalysis Using Linear Free Energy Relationships. *Angew. Chem. Int. Ed.* **2008**, *47*, 771-774; (d) Pothupitiya, J. U.; Hewawasam, R. S.; Kiesewetter, M. K. Urea and Thiourea H-Bond Donating Catalysts for Ring-Opening Polymerization: Mechanistic Insights via (non) Linear Free Energy Relationships. *Macromolecules* **2018**, *51*, 3203-3211; (e) Lan, Z.; Sharada, S. M. A Framework for Constructing Linear Free Energy Relationships to Design Molecular Transition Metal Catalysts. *Phys. Chem. Chem. Phys.* **2021**, *23*, 15543-15556.
8. (a) Kreevoy, M. M.; Lee, I. S. H. Marcus Theory of a Perpendicular Effect on α for Hydride Transfer Between NAD^+ Analogs. *J. Am. Chem. Soc.* **1984**, *106*, 2550-2553; (b) Ostovic, D.; Lee, I. S. H.; Roberts, R. M. G.; Kreevoy, M. M. Hydride Transfer and Oxyanion Addition Equilibria of NAD^+ Analogs. *J. Org. Chem.* **1985**, *50*, 4206-4211; (c) Kreevoy, M. M.; Ostovic, D.; Lee, I. S. H.; Binder, D. A.; King, G. W. Structure Sensitivity of the Marcus λ Parameter for Hydride Transfer Between NAD^+ Analogs. *J. Am. Chem. Soc.* **1988**, *110*, 524-530; (d) Kim, Y.; Truhlar, D. G.; Kreevoy, M. M. An Experimentally Based Family of Potential Energy Surfaces for Hydride Transfer Between NAD^+ Analogs. *J. Am. Chem. Soc.* **1991**, *113*, 7837-7847; (e) Lee, I.-S. H.; Jeoung, E. H.; Kreevoy, M. M. Marcus Theory of a Parallel Effect on α for Hydride Transfer Reaction between NAD^+ Analogues. *J. Am. Chem. Soc.* **1997**, *119*, 2722-2728; (f) Han Lee, I.-S.; Jeoung, E. H.; Kreevoy, M. M. Primary Kinetic Isotope Effects on Hydride Transfer from 1,3-Dimethyl-2-phenylbenzimidazoline to NAD^+ Analogues. *J. Am. Chem. Soc.* **2001**, *123*, 7492-7496; (g) Mayr, H.; Bug, T.; Gotta, M. F.; Hering, N.; Irrgang, B.; Janker, B.; Kempf, B.; Loos, R.; Ofial, A. R.; Remennikov, G.; Schimmel, H. Reference Scales for the Characterization of Cationic Electrophiles and Neutral Nucleophiles. *J. Am. Chem. Soc.* **2001**, *123*, 9500-9512; (h) Minegishi, S.; Kobayashi, S.; Mayr, H. Solvent Nucleophilicity. *J. Am. Chem. Soc.* **2004**, *126*, 5174-5181; (i) Lee, I.-S. H.; Chow, K.-H.; Kreevoy, M. M. The Tightness Contribution to the Brønsted α for Hydride Transfer between NAD^+ Analogues. *J. Am. Chem. Soc.* **2002**, *124*, 7755-7761; (j) Dichiarante, V.; Fagnoni, M.; Albini, A. Using Phenyl Cations as Probes for Establishing Electrophilicity-Nucleophilicity Relations. *J. Org. Chem.* **2008**, *73*, 1282-1289; (k) Um, I.-H.; Im, L.-R.; Kang, J.-S.; Bursey, S. S.; Dust, J. M. Mechanistic Assessment of SN_{Ar} Displacement of Halides from 1-Halo-2,4-dinitrobenzenes by Selected Primary and Secondary Amines: Brønsted and Mayr Analyses. *J. Org. Chem.* **2012**, *77*, 9738-9746; (l) Alherz, A.; Lim, C.-H.; Hynes, J. T.; Musgrave, C. B. Predicting Hydride Donor Strength via Quantum Chemical Calculations of Hydride Transfer Activation Free Energy. *J. Phys. Chem. B* **2018**, *122*, 1278-1288.
9. (a) Weerasooriya, R. B.; Gesiorski, J. L.; Alherz, A.; Ilic, S.; Hargenrader, G. N.; Musgrave, C. B.; Glusac, K. D. Kinetics of Hydride Transfer from Catalytic Metal-Free Hydride Donors to CO_2. *J. Phys. Chem. Lett.* **2021**, *12*, 2306-2311; (b) Ilic, S.; Gesiorski, J. L.; Weerasooriya, R. B.; Glusac, K. D. Biomimetic Metal-Free Hydride Donor Catalysts for CO_2 Reduction. *Acc. Chem. Res.* **2022**, *55*, 844-856.
10. Jeletic, M. S.; Hulley, E. B.; Helm, M. L.; Mock, M. T.; Appel, A. M.; Wiedner, E. S.; Linehan, J. C. Understanding the Relationship Between Kinetics and Thermodynamics in CO_2 Hydrogenation Catalysis. *ACS Catal.* **2017**, *7*, 6008-6017.
11. Ngo, A. H.; Do, L. H. Structure–Activity Relationship Study of Half-Sandwich Metal Complexes in Aqueous Transfer Hydrogenation Catalysis. *Inorg. Chem. Front.* **2020**, *7*, 583-591.
12. Matsubara, Y.; Fujita, E.; Doherty, M. D.; Muckerman, J. T.; Creutz, C. Thermodynamic and Kinetic Hydricity of Ruthenium(II) Hydride Complexes. *J. Am. Chem. Soc.* **2012**, *134*, 15743-15757.

13. (a) Sarker, N.; Bruno, J. W. Thermodynamic and Kinetic Studies of Hydride Transfer for a Series of Molybdenum and Tungsten Hydrides. *J. Am. Chem. Soc.* **1999**, *121*, 2174-2180; (b) Cheng, T.-Y.; Bullock, R. M. Hydride Transfer from (η^5-C_5Me_5)$(CO)_2$MH (M = Fe, Ru, Os) to Trityl Cation: Different Products from Different Metals and the Kinetics of Hydride Transfer. *Organometallics* **2002**, *21*, 2325-2331.
14. Ellis, W. W.; Raebiger, J. W.; Curtis, C. J.; Bruno, J. W.; DuBois, D. L. Hydricities of BzNADH, $C_5H_5Mo(PMe_3)(CO)_2H$, and $C_5Me_5Mo(PMe_3)(CO)_2H$ in Acetonitrile. *J. Am. Chem. Soc.* **2004**, *126*, 2738-2743.
15. Nijamudheen, A.; Kanega, R.; Onishi, N.; Himeda, Y.; Fujita, E.; Ertem, M. Z. Distinct Mechanisms and Hydricities of Cp*Ir-Based CO_2 Hydrogenation Catalysts in Basic Water. *ACS Catal.* **2021**, *11*, 5776-5788.
16. Another way of expressing that the range of hydride acceptor abilities was narrow, is that the conjugate hydricities of the acceptors were limited. See reference 6e for a discussion of conjugate hydricity.
17. Sullivan, B. P.; Meyer, T. J. Kinetics and Mechanism of Carbon Dioxide Insertion into a Metal-Hydride Bond. A Large Solvent Effect and an Inverse Kinetic Isotope Effect. *Organometallics* **1986**, *5*, 1500-1502.
18. By outer-sphere mechanism we mean that there is no interaction between the metal and CO_2 in the rate-determining transition state. Instead the key interaction is between the nucleophilic hydride and the electrophilic carbon center of CO_2.
19. (a) Schmeier, T. J.; Dobereiner, G. E.; Crabtree, R. H.; Hazari, N. Secondary Coordination Sphere Interactions Facilitate the Insertion Step in an Iridium(III) CO_2 Reduction Catalyst. *J. Am. Chem. Soc.* **2011**, *133*, 9274-9277; (b) Schmeier, T. J.; Hazari, N.; Incarvito, C. D.; Raskatov, J. A. Exploring the Reactions of CO_2 with PCP Supported Nickel Complexes. *Chem. Commun.* **2011**, *47*, 1824-1826; (c) Suh, H.-W.; Schmeier, T. J.; Hazari, N.; Kemp, R. A.; Takase, M. K. Experimental and Computational Studies of the Reaction of Carbon Dioxide with Pincer-Supported Nickel and Palladium Hydrides. *Organometallics* **2012**, *31*, 8225-8236; (d) Ríos, P.; Rodríguez, A.; López-Serrano, J. Mechanistic Studies on the Selective Reduction of CO_2 to the Aldehyde Level by a Bis(phosphino)boryl (PBP)-Supported Nickel Complex. *ACS Catal.* **2016**, *6*, 5715-5723; (e) Hazari, N.; Heimann, J. E. Carbon Dioxide Insertion into Group 9 and 10 Metal–Element σ Bonds. *Inorg. Chem.* **2017**, *56*, 13655-13678; (f) Heimann, J. E.; Bernskoetter, W. H.; Hazari, N.; Mayer, J. M. Acceleration of CO_2 Insertion into Metal Hydrides: Ligand, Lewis Acid, and Solvent Effects on Reaction Kinetics. *Chem. Sci.* **2018**, *9*, 6629-6638; (g) Heimann, J. E.; Bernskoetter, W. H.; Hazari, N. Understanding the Individual and Combined Effects of Solvent and Lewis Acid on CO_2 Insertion into a Metal Hydride. *J. Am. Chem. Soc.* **2019**, *141*, 10520-10529.
20. (a) Jaffé, H. H. A Reexamination of the Hammett Equation. *Chem. Rev.* **1953**, *53*, 191-261; (b) Leo, C. H. A. *Substituent Constants for Correlation Analysis in Chemistry and Biology*; John Wiley & Sons, Ltd: Toronto, 1979; (c) Hansch, C.; Leo, A.; Taft, R. W. A Survey of Hammett Substituent Constants and Resonance and Field Parameters. *Chem. Rev.* **1991**, *91*, 165-195.
21. Brereton, K. R.; Jadrich, C. N.; Stratakes, B. M.; Miller, A. J. M. Thermodynamic Hydricity Across Solvents: Subtle Electronic Effects and Striking Ligation Effects in Iridium Hydrides. *Organometallics* **2019**, *38*, 3104-3110.
22. (a) Kao, S. C.; Spillett, C. T.; Ash, C.; Lusk, R.; Park, Y. K.; Darensbourg, M. Y. Relative Reactivity and Mechanistic Studies of the Hydride-Transfer Reagents $HM(CO)_4L$-(M = Cr, W; L = CO, PR_3). *Organometallics* **1985**, *4*, 83-91; (b) Cheng, T.-Y.; Brunschwig, B. S.; Bullock, R. M. Hydride Transfer Reactions of Transition Metal Hydrides: Kinetic Hydricity of Metal Carbonyl Hydrides. *J. Am. Chem. Soc.* **1998**, *120*, 13121-13137.
23. A list of hydride acceptors that did not provide clean reactivity is provided in the SI.
24. Ilic, S.; Pandey Kadel, U.; Basdogan, Y.; Keith, J. A.; Glusac, K. D. Thermodynamic Hydricities of Biomimetic Organic Hydride Donors. *J. Am. Chem. Soc.* **2018**, *140*, 4569-4579.
25. Yang, X.; Walpita, J.; Zhou, D.; Luk, H. L.; Vyas, S.; Khnayzer, R. S.; Tiwari, S. C.; Diri, K.; Hadad, C. M.; Castellano, F. N.; Krylov, A. I.; Glusac, K. D. Toward Organic Photohydrides: Excited-State Behavior of 10-Methyl-9-phenyl-9,10-dihydroacridine. *J. Phys. Chem. B* **2013**, *117*, 15290-15296.
26. Zhang, X.-M.; Bruno, J. W.; Enyinnaya, E. Hydride Affinities of Arylcarbenium Ions and Iminium Ions in Dimethyl Sulfoxide and Acetonitrile. *J. Org. Chem.* **1998**, *63*, 4671-4678.
27. (a) Berning, D. E.; Noll, B. C.; DuBois, D. L. Relative Hydride, Proton, and Hydrogen Atom Transfer Abilities of $[HM(diphosphine)_2]PF_6$ Complexes (M = Pt, Ni). *J. Am. Chem. Soc.* **1999**, *121*, 11432-11447; (b) DuBois, D. L.; Berning, D. E. Hydricity of Transition-Metal Hydrides and its Role in CO_2 Reduction. *Appl. Organomet. Chem.* **2000**, *14*, 860-862; (c) Miller, A. J. M.; Labinger, J. A.; Bercaw, J. E. Trialkylborane-Assisted CO_2 Reduction by Late Transition Metal Hydrides. *Organometallics* **2011**, *30*, 4308-4314.
28. Two alternative explantions relate to the smaller size of CO_2. In the first, because CO_2 is smaller it can approach Re more efficiently and therefore generate more order. In the second, the contribution of translational entropy to the overall entropy is likely very different for CO_2 because there are significantly less degrees of freedom given that CO_2 contains fewer atoms than the cationic N-heterocyclic acceptors.

29. Cheng, T.-Y.; Bullock, R. M. Isotope Effects on Hydride Transfer Reactions from Transition Metal Hydrides to Trityl Cation. An Inverse Isotope Effect for a Hydride Transfer. *J. Am. Chem. Soc.* **1999**, *121*, 3150-3155.
30. This is further supported by the increase in the enthalpy of activation as the thermodynamic driving force decreases, suggesting increased cleavage of the metal hydride bond when the acceptor has a lower hydride affinity.
31. Mathis, C. L.; Geary, J.; Ardon, Y.; Reese, M. S.; Philliber, M. A.; VanderLinden, R. T.; Saouma, C. T. Thermodynamic Analysis of Metal–Ligand Cooperativity of PNP Ru Complexes: Implications for CO_2 Hydrogenation to Methanol and Catalyst Inhibition. *J. Am. Chem. Soc.* **2019**, *141*, 14317-14328.
32. We note that the favorability of formate binding to different complexes of the type $[Re(^{R}bpy)(CO)_3(ACN)]^+$ changes depending on the substituent on the bpy. Therefore, the effective thermodynamic hydride affinity of CO_2 varies depending on the substituent on the bpy. However, this change is small and for the sake of simplicity we have exclusively used the energy of formate binding to the unsubstituted complex $[Re(^{R}bpy)(CO)_3(ACN)]^+$ to calculate the effective thermodynamic hydride affinity of CO_2 in this manuscript.
33. This hypothesis is supported by previous work which demonstrates that deviations in the linear relationship between the rate of proton transfer from organic acids to a metal and the pKa of the acid are caused by changes in steric properties. See the following reference for more information: Elgrishi, N.; Kurtz, D. A.; Dempsey, J. L. Reaction Parameters Influencing Cobalt Hydride Formation Kinetics: Implications for Benchmarking H_2-Evolution Catalysts. *J. Am. Chem. Soc.* **2017**, *139*, 239-244.
34. Clark, M. L.; Cheung, P. L.; Lessio, M.; Carter, E. A.; Kubiak, C. P. Kinetic and Mechanistic Effects of Bipyridine (bpy) Substituent, Labile Ligand, and Brønsted Acid on Electrocatalytic CO_2 Reduction by Re(bpy) Complexes. *ACS Catal.* **2018**, *8*, 2021-2029.
35. Zhao, Y.; Truhlar, D. G. The M06 Suite of Density Functionals for Main Group Thermochemistry, Thermochemical Kinetics, Noncovalent Interactions, Excited States, and Transition Elements: Two New Functionals and Systematic Testing of Four M06-Class Functionals and 12 Other Functionals. *Theor. Chem. Acc.* **2008**, *120*, 215-241.
36. Weigend, F.; Ahlrichs, R. Balanced Basis Sets of Split Valence, Triple Zeta Valence and Quadruple Zeta Valence Quality for H to Rn: Design and Assessment of Accuracy. *Phys. Chem. Chem. Phys.* **2005**, *7*, 3297-3305.
37. Marenich, A. V.; Cramer, C. J.; Truhlar, D. G. Universal Solvation Model Based on Solute Electron Density and on a Continuum Model of the Solvent Defined by the Bulk Dielectric Constant and Atomic Surface Tensions. *J. Phys. Chem. B* **2009**, *113*, 6378-6396.
38. (a) Riplinger, C.; Neese, F. An Efficient and Near Linear Scaling Pair Natural Orbital Based Local Coupled Cluster Method. *J. Chem. Phys.* **2013**, *138*, 034106; (b) Riplinger, C.; Sandhoefer, B.; Hansen, A.; Neese, F. Natural Triple Excitations in Local Coupled Cluster Calculations with Pair Natural Orbitals. *J. Chem. Phys.* **2013**, *139*, 134101.
39. (a) Ahlquist, M. S. Iridium Catalyzed Hydrogenation of CO_2 Under Basic Conditions–Mechanistic Insight From Theory. *J. Mol. Catal. A: Chem.* **2010**, *324*, 3-8; (b) Osadchuk, I.; Tamm, T.; Ahlquist, M. r. S. Theoretical Investigation of a Parallel Catalytic Cycle in CO_2 Hydrogenation by (PNP)IrH_3. *Organometallics* **2015**, *34*, 4932-4940; (c) Mondal, B.; Neese, F.; Ye, S. Control in the Rate-Determining Step Provides a Promising Strategy to Develop New Catalysts for CO_2 Hydrogenation: A Local Pair Natural Orbital Coupled Cluster Theory Study. *Inorg. Chem.* **2015**, *54*, 7192-7198; (d) Li, J.; Liu, S.; Lu, X. Theoretical Study of the Mechanism for Direct Addition of Hydride to CO_2 on Ruthenium Complexes: Nature of Ru–H Bond and Effect of Hydrogen Bonding. *Bull. Chem. Soc. Jpn.* **2016**, *89*, 905-910; (e) Ono, T.; Qu, S.; Gimbert-Surinach, C.; Johnson, M. A.; Marell, D. J.; Benet-Buchholz, J.; Cramer, C. J.; Llobet, A. Hydrogenative Carbon Dioxide Reduction Catalyzed by Mononuclear Ruthenium Polypyridyl Complexes: Discerning Between Electronic and Steric Effects. *ACS Catal.* **2017**, *7*, 5932-5940.
40. Agarwal, J.; Johnson, R. P.; Li, G. Reduction of CO_2 on a Tricarbonyl Rhenium(I) Complex: Modeling a Catalytic Cycle. *J. Phys. Chem. A* **2011**, *115*, 2877-2881.
41. In the Supporting Information we have provided the classical Marcus plots of $\ln(k_1)$ versus ΔG^o for hydride transfer for each of our Re hydrides to the different acceptors.
42. Yuasa, J.; Fukuzumi, S. A Mechanistic Dichotomy in Concerted Versus Stepwise Pathways in Hydride and Hydrogen Transfer Reactions of NADH Analogues. *J. Phys. Org. Chem.* **2008**, *21*, 886-896.

TOC Graphic

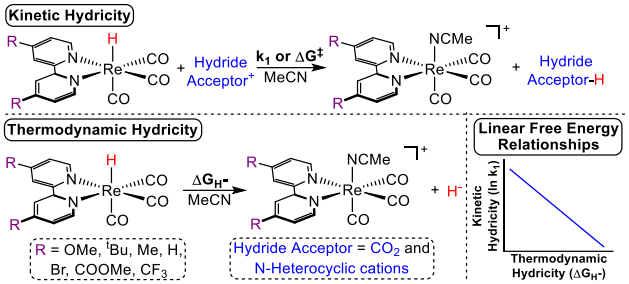
Kinetic Hydricity
Hydride Acceptor+
k1 or ΔG‡
MeCN
NCMe
Hydride Acceptor-H
Thermodynamic Hydricity
ΔGH-
MeCN
+ H-
R = OMe, tBu, Me, H, Br, COOMe, CF3
Hydride Acceptor = CO2 and N-Heterocyclic cations
Linear Free Energy Relationships
Kinetic Hydricity (ln k1)
Thermodynamic Hydricity (ΔGH-)